ER ID 97871

SOIL VAPOR EXTRACTION PILOT TEST AT TECHNICAL AREA 54, MATERIAL DISPOSAL AREA L: NUMERICAL MODELING IN SUPPORT OF DECISION ANALYSIS

Philip H. Stauffer
Mail Stop T-003
Los Alamos National Laboratory
Los Alamos NM, 87545

John K. Hopkins
Mail Stop M-992
Los Alamos National Laboratory
Los Alamos NM, 87545

Tom Anderson
Apogen Technologies
1350 Central Ave.
Los Alamos NM, 87544

Jasper Vrugt
Mail Stop T-003
Los Alamos National Laboratory
Los Alamos NM, 87545

I. ABSTRACT

This report presents a numerical model of an SVE pilot test on a volatile organic compound (VOC) plume in the subsurface at Material Disposal Area L, Los Alamos National Laboratory. A site-scale numerical model was previously developed to evaluate the impact of subsurface processes on subsurface contaminants associated with waste disposed at the site. One of the main goals of the SVE modeling is to support the corrective measures evaluation. The model has been extensively tested and used to confirm our conceptual model for transport within the very dry mesa-top setting. In this study we present results of simulations of the SVE test. The SVE simulations are performed on a new high resolution, 3-D, site scale model. The model is calibrated to the extraction borehole concentration data using a state-of-the-art single objective optimization algorithm. Simulations show how the site may behave in the event of a sudden release of VOC from subsurface drums. Results show that the current monitoring network should be able to detect sudden VOC release of 800-1400 kg within one year. Subsequent simulations of SVE show that the current two SVE boreholes at the site would likely be sufficient to remove a substantial portion of the total sudden release within a one year period. The simulations show that some modification to the current system may be required to extract VOC from deeper in the mesa, such as installation of two new SVE holes with casing to greater depth. Plume rebound calculations suggest that in the absence of a catastrophic leak, the SVE system would only need to be operated for two to three months in each one to three year period. Finally, the simulated radius of influence is greatest in the higher permeability units, and for practical purposes extends to approximately 40 m.

LA-UR-07-4890

30765

II. INTRODUCTION

The SVE Pilot test at the Los Alamos National Laboratories former liquid waste disposal area, MDA L was designed to collect data to better understand how vapor extraction technology could used in the corrective measures analysis and possible future remediation. MDA L is located just north of Pajarito Rd., about 3 km west of the town of White Rock. The site is on top of Mesita del Buey, a finger mesa that is bounded to the north by Canada del Buey and to the south by Pajarito Canyon. Figure 1 shows an aerial photograph of MDA L (outlined by an orange line), surrounding boreholes, and the locations of the shafts and pits in which liquid waste was disposed of during the time period that this site was an active subsurface disposal unit. This figure also shows the locations of the two pilot SVE wells (red circles) that were used to extract subsurface vapor during the tests. The red circle on the left of the figure marks the location of SVE West and the one on the right marks the location of SVE East. The site is currently being used as an above ground packaging and storage facility for chemical waste as can be seen by the buildings and pavement that cover the site.

This paper is a continuation of a previous numerical modeling work on a VOC plume located beneath the former Los Alamos National Laboratories liquid waste disposal area, MDA L. The first of the previous papers, Stauffer et al. [35] presented a numerical model of plume growth from the years 1975 – 2000 that was used to constrain processes in the conceptual model of diffusive transport within the mesa on which MDA L is located. This model was calibrated using a set of 132 borehole vapor measurements of 1,1,1 trichlorethane (TCA), the primary volatile organic compound (VOC) at MDA L. The simulations were performed using a finite volume heat and mass transport code (FEHM) that solves the diffusion equation and includes Henry's Law partitioning between the liquid and vapor phases [21]. The calculations were performed on a numerical grid that incorporates local topography and honors existing knowledge of subsurface geology in three dimensions. Results from this modeling exercise allowed us to refine our conceptual model for plume growth at this site. We believe that the source release is most likely characterized by slow leaking of TCA vapor leading to relatively constant source region TCA concentrations in the range of 3000 ppmv, well below the saturated vapor pressure of 160,000 ppmv that would be seen when TCA vapor is in equilibrium with a liquid source. Transport away from the source region is primarily by diffusion, with model diffusion coefficients falling very close to values measured on core samples from the site. This implies that barometric pumping and wind effects are not effective in increasing the in situ diffusion of TCA. Furthermore, the inclusion of Henry's Law partitioning between the liquid and vapor phases was required to achieve the best fit. Finally, the asphalt at the site appears to be acting as a diffusive barrier, leading to a broader plume within the subsurface and higher concentrations in the shallow subsurface near the source region.

The second paper that we build on, Stauffer et al. [35], presents preliminary analysis of the SVE tests using both two and three dimensional numerical models. This work suggested that the subsurface most likely behaves as a dual continuum during the SVE test, with higher permeability conduits and lower permeability regions contributing to the total air flow that is captured by the extraction wells. The effective porosity of the higher permeability pathways is on the order of 10 – 15%. Because traditional fractures have a porosity of only 0.1% or less, this implies that fractures are most likely not well connected over large distance yet provided

increased local permeability. However, the long term extraction tail can be fit with a single continuum, and Section 2.3.4 in the current paper presents logic that reduces the probable role of dual continuum behavior and helps to explain some of the inconsistencies found in the data. Another result presented in Stauffer et al. [35] was to show that our new, high resolution numerical grid is able to recreate the results of the original coarse grid for plume growth through the year 2000. The new grid is vital to the SVE study because it allows much finer resolution of concentrations and pressures in the upper 90 m where the effects of the SVE vacuum are most pronounced.

We take the results from the two previous modeling papers and use these as the foundation for the current study that is broken into three main sections. In Section 1 we review model details including both the conceptual and numerical models of flow and transport. Next, we discuss automated 3-D model calibration, done since the release of Stauffer et al. [35], that uses thousands of simulations to better match concentrations in the extraction wellbores. This section includes a discussion of possible problems with the FLUTE system that may require us to reexamine short term data from boreholes surrounding the SVE extraction holes. Finally, in Section 3 we present results of hypothetical sudden releases at both the East and West source areas. We show how quickly the releases are expected to be seen in the nearby monitoring wells, and then show how the released TCA responds to the SVE system. Additional topics discussed include the rebound of the plume due to continued slow leakage from the source region and the consequences of not remediating both the sudden release scenario and the continued slow leak.

1. MODEL DISCUSSION

1.1. Vadose zone transport properties

This section describes the physical properties that are relevant for the SVE modeling. Table I lists physical properties relevant for TCA transport. Table II lists the mean measured porosity, saturation, and effective diffusion coefficient determined from the best-fit model. Table III lists measured air permeability ranges for the geologic units beneath the site (Figure 2) for both straddle packer measurements and core measurements. The straddle packer permeability measurements were made on seven boreholes found approximately 100 m to the east of the MDA L boudnary. The packer interval was 0.6 m (2ft) and the data provide a high resolution view of variability that is typical of the Bandelier Tuff. Straddle packer measurements were not made in the SVE boreholes used for the MDA L Pilot Test, thus the measured values provide the best initial guess as to the likely range of values expected around the SVE holes. The mean core permeability measurements are generally at least an order of magnitude lower than the mean straddle packer measurements, showing the role that fractures play in the rocks at MDA L. The permeability data show that increased permeability due to fractures at this site is not limited to the more welded Units Qbt-2 and Qbt-1vc, but is apparently ubiquitous throughout the Tshirege member of the Bandelier Tuff.

1.2. Concentration units used in the Calibration

Historically at MDA L, vapor concentrations have been reported in units of ppmv, meaning parts per million by volume. This is equivalent to one million times the ratio of the number of moles of a contaminant to the total number of moles in a given volume. The units of ppmv are quite useful in that the measured value in a given packet of air will not change in response to changes in pressure or temperature. Therefore as air expands or contracts, the ppmv concentration will

remain constant. Recently, the New Mexico Environmental department has requested that VOC concentrations be reported in units of ug/m3. This is somewhat problematic because when one converts samples measured in ug/m3 to ppmv, samples of different densities, caused by changes in pressure and temperature, will yield different values of concentration. Because concentration gradients are what drive diffusive transport, it is important to limit the error in the measured values. This is especially problematic because generally the pressure and temperature of the sample are not reported. For example, if soil gas is pulled to the surface for measurement where the temperature is significantly less than in the subsurface, the measured values will be higher by the ratio of density between the cold gas and the warmer gas in the subsurface. The density difference for air between 0 C and 30 C leads to a difference in calculated ug/m3 of about 10%.

To convert between the two units, one must know the molecular weight of the contaminant and that of air. Air is a mixture of many gasses, but can be approximated as having a molecular weight of 29 g/mol. The primary VOC at MDA L, TCA, has a molecular weigh of 133 g/m (Table I). Assuming that the density of air on the mesa top elevation and temperature of 2072 m and 10 C (6800 ft and 50 F) is approximately 1 kg/m^3, a concentration of 1000 ppmv TCA can be converted to ug/m^3 as:

$$1000 \text{ ppmv} = 1000 \text{ moles TCA}/1e6 \text{ moles Air}$$

$$1000 \text{ moles TCA} * 133 \text{ g/mol} * 1e6 \text{ ug/g} = 133.e9 \text{ ug TCA}$$
$$1e6 \text{ moles Air} * 29 \text{ g/mol} * 1 \text{ m}^3\text{/kg} = 29000 \text{ m}^3$$
$$\text{Yielding}$$
$$133.e9 \text{ ug}/29000 \text{ m}^3 = 4.6e6 \text{ ug/m}^3$$

1.3. Conceptual model

1.3.1. Processes included in the conceptual model

The conceptual model for plume growth at MDA L is described in Stauffer et al. [7], and we summarize the assumptions and findings of that study in this paragraph. These findings form the basis for the conceptual model used in the current paper. The primary VOC in the plume, comprising approximately 70% by mass of the total plume, TCA, is taken as representative of the plume. The VOC plume MDA L is controlled by vapor diffusion through variably saturated rocks with partitioning into the liquid phase. A zero concentration atmospheric boundary following the topography of the mesa and canyon is necessary to simulate the current plume. The rock saturation and porosity limit the ability of vapor to diffuse and the numerical representation of an effective diffusion coefficient are described below in the Model Formulation section. Henry's Law partitioning between the vapor and liquid phases (also described in the Model Formulation section) and greatly reduced diffusion across the asphalt at the site are both very important at MDA L. The best-fit land/air interface diffusion coefficient is slightly lower than the value used for the surface rocks, to represent the effects of a soil horizon that may contain more water than is found in the deeper mesa. Finally, the plume appears to be in a pseudo-steady state, growing only slowly, because most of the source release is following steep concentration gradients toward the atmosphere.

In this paper, we make the further assumption that during SVE, TCA transport can be described by the advection-dispersion equation [see Section 1.3]. The role of fractures appears to be quite

important for simulating the concentration rebounds in the SVE tests [35]. Rocks containing fractures and porous rock matrix form a dual continuum that can behave differently than rocks containing only a single continuum of porous rock [6]. At this site, the rocks in Qbt2 and Qbt1-vc contain numerous vertical fractures that can lead to significant increases in permeability (Table III). Robinson et al. [19] found that water injection in the Bandelier Tuff showed behavior that was best fit with a single continuum representative of the matrix; however, air flow is substantially different from water flow due to capillary suction that pulls water into pores. Additionally, as described in the vadose zone transport section (1.1), the straddle packer data show much higher air permeability than the core data for all units tested.

Pipe flow can lead to frictional losses, however calculations done on a pipe flow calculator (web based: www.efunda.com/formulas) for an 8 inch diameter pipe with values of density, viscosity, and flow rate appropriate for the SVE tests show that such losses should be quite small, less than 10 Pa in 65 ft (19.8 m). Because the SVE tests generated suction of greater than 10 kPa, we ignore the effects of frictional losses in the boreholes, and set the borehole permeability high enough (1.0×10^{-4} m^2) to ensure a pressure drop of less than 30 Pa.

Currently, the 3-D site scale model cannot incorporate dual continuum behavior; however the results of calibrated simulations presented should be fairly robust in capturing the general behavior of the system. This is because the full porosity can be assigned an equivalent permeability that will recreate the pressure-flow rate response at the wellhead. Although this approximation will not reproduce the steep drop-off in concentrations seen in the data or the rebound spikes seen after SVE shut-in, the long term evolution of the plume should be of the correct magnitude and spatial extent. We stress that this would not be the case if the matrix permeability was several orders of magnitude lower; however with the high matrix permeabilities measured in the Bandelier Tuff (Table III), equilibration times between matrix and fractures should be significantly shorter than those found in dual continua such as clay/sand systems where contaminant tails can last for decades due to diffusion limited mass removal from extremely low permeability clays (Fetter, 1999). Additionally, Section 2.3.4 points out some possible inconsistencies in the rebound and manometer data that seem to imply that a single continuum may be sufficient to simulate the SVE Pilot test.

1.3.2. Processes not included in the conceptual model

Movement of liquid water at this site is assumed to be negligible (<1 mm/yr) and arguments for this assumption can be found in the conceptual model for flow and transport of liquid water beneath the Pajarito Plateau [20]. Temperatures vary only by a few degrees C within the region of interest in the mesa and we assume isothermal conditions for all simulations presented. Because measured effective diffusion coefficients of TCE on crushed tuff columns were very similar to those required to best fit the plume growth [15], we assume that barometric pumping within the mesa is not leading to increased apparent diffusion. Although the land/air interface in the previous model used a slightly lower effective diffusion coefficient, in the current model we do not reduce the permeability at this interface. Such a minor reduction in properties should have very little impact on the SVE simulations because the SVE system is much more sensitive to the properties of the rocks within the mesa that are in contact with the open interval of the extraction boreholes.

1.4. Model formulation

We are using the Los Alamos porous flow simulator, FEHM, for all calculations presented in this paper [21,37]. FEHM is a finite-volume heat and mass transfer code that has been used extensively for simulation of multiphase transport [22, 23, 24, 25, 7, 26]. Equations governing the conservation of phase mass, contaminant moles, and energy are solved numerically using a fully implicit Newton-Raphson scheme. As stated in the conceptual model section, we simplify the analysis by assuming constant temperature and no movement of the liquid phase. Justification for these assumptions in the context of the Pajarito Plateau is given in Stauffer et al. [7]. Further, we assume that the atmospheric pressure on the top of the mesa at an elevation of 2072 masl (6798 feet above sea level) is constant at 80 kPa.

The primary assumptions governing vapor-phase flow and transport are as follows. First, we assume that the vapor phase is composed solely of air that obeys the Ideal Gas Law and calculate vapor-phase density (kg/m^3) as a function of vapor pressure, P_v (MPa), and temperature, T (C) as:

$$\rho_v = 1.292864\left(\frac{273.15}{T+273.15}\right)\left(\frac{P_v}{0.101325}\right) \qquad \text{Eq. 1}$$

We use Darcy's law to calculate the advective volume flux [27] of the vapor phase as:

$$v_v = -\frac{kR_v}{\mu_v}(\nabla P_v - \rho_v \bar{g}) \qquad \text{Eq. 2}$$

where k is the intrinsic permeability of the rock (m^2), R_v is the relative permeability function for the vapor phase (calculated as a function of saturation via a Brooks-Corey relationship for this study [28]), $\bar{g}$ is the gravitational vector (9.81 m^2/s), and vapor viscosity is assumed constant as:

$$\mu_v = 1.82x10^{-5}\, Pa \cdot s \qquad \text{Eq. 3}$$

Vapor-phase contaminant conservation is governed by the advection-dispersion equation (Fetter, 1999) where the contaminant flux (moles/(m^2 s))is given by:

$$q_v = v_v C_v + \phi S_v D^i{}_{cv} \cdot \nabla C_v \qquad \text{Eq. 4}$$

where ϕ is porosity, S_v is vapor saturation defined as air filled porosity divided by total porosity, C_v is the molar concentration (moles/m$^3{}_{phase}$) and the dispersion coefficient, D_{cv}, includes contributions from both dispersivity (and molecular diffusion as:

$$D_{cv} = \alpha^i (v^i{}_v / \phi) + D^*{}_v \qquad \text{Eq. 5}$$

where the molecular diffusion coefficient in FEHM is a function of the free air diffusion coefficient (D_{free}) and the tortuosity (τ) as:

$$D^*{}_v = \tau D_{free} \qquad \text{Eq. 6}$$

The dispersivity tensor (α^i) is directional; however in FEHM we keep only the diagonal terms of this tensor. The superscript i implies that the equation is solved for the principle directions. For example, in 3-D, the volume flux at any point can be decomposed into three principle

components, v_x, v_y, and v_z, while in 2-D radial the components are v_r and v_z. An additional constraint is imposed by Henry's Law equilibrium partitioning which requires a constant ratio between concentrations in the liquid and vapor phase as:

$$C_v = HC_l \qquad \text{Eq. 7}$$

where the Henry's Law value for TCA (H_{TCA}) is listed in Table I. As described, the model is a molar based solution to the advection-dispersion equation using Fickian transport theory. We do not account for the effects of non-Fickian diffusion; however corrections for non-equimolar behavior are relatively small (<3%) [29].

FEHM also has a new capability that allows us to embed radial boreholes within an existing 3-D site scale mesh [32]. This capability is used to reduce the total number of nodes required to capture the radial flow near the simulated SVE extraction holes while also capturing the topography and stratigraphy at the site scale. Without this capability, we would need to embed two 3-D extraction borehole meshes and all the necessary extra nodes to allow the borehole meshes to correctly connect to the existing 3-D grid while maintaining the Voronoi volume constraints that are required for computational accuracy. Furthermore, the flexibility allowed by the new capability is such that one can add or remove boreholes at any time, permitting us to study the effects of SVE borehole placement location without having to spend large amounts of time embedding 3-D borehole meshes into site scale grids. Another useful feature of the wellbore capability includes the ability to add onion shells around the open hole, allowing us to include a very low permeability casing that correctly simulates the in situ casing used for the SVE Pilot Tests. Currently, use of the wellbore module precludes the use of the dual continuum portion of the code; however, we are working to allow simultaneous use of both options. As stated previously in Section 1.2.1, we believe that omission of the dual continuum behavior of the system results in some mismatch between model and data during rebound spikes; however we should be able to capture the long term behavior of the plume by using an equivalent continuum approximation.

1.5. 3-D Model domain and computational grid

1.5.1. Numerical grid

The 3-D simulation domain is approximately centered on MDA L, and includes the surrounding mesa/canyon environment from the land surface to the water table. Figure 4 shows an aerial photo of MDA L with the computational domain outlined in red. This figure also shows contours of the initial plume on a horizontal plane sliced 80 ft below the surface of the mesa. MDA L is approximately 180 m E-W by 120 m N-S (600 x 400 ft), and the simulated domain extends beyond the site on all sides by a minimum of 100 m to minimize boundary effects. The computational grid is made up of over 140,000 nodes and nearly 800,000 volume elements. The lateral extent is 410. m E-W by 370 m N-S. The grid extends vertically from an elevation of 1737 meters above sea level (masl) at the water table to 2074 masl on the northwestern corner of Mesita del Buey. The grid has a vertical resolution of 1 m in the top 90 m and stretches to a resolution of 25 m at the water table. The horizontal resolution of the primary grid is everywhere 10 m. The grid captures the topography of the site and extends to the water table, over 300 m below the surface of the mesa on which MDA L is situated. The deeper part of the grid, 270 ft (90 m) below the mesa top, has little impact on the simulations, and is included to address questions concerning plume impacts on the regional water table. The 3-D grid used in this paper

is an extension and refinement of the grid used in Stauffer et al. [7]. Figure 5 and Figure 6 show two additional views of the 3-D domain. Figure 5 is an angled view of the entire simulation block showing the gross stratigraphy. Figure 6 shows two slice planes of the pre-SVE plume concentrations, one on the same plane 80 ft below the surface shown in Figure 4, and another vertical slice along the axis of the mesa. The high resolution embedded wellbores used in the simulations each have an inner radius of 0.08 m and an outer shell radius of 2 m with 4 nodes spanning this distance. Therefore each well has one vertical line of nodes representing the open hole and four onion skins surrounding this. Both SVE holes have a total depth of 66 m (216 ft) with 67 nodes along the vertical. The nodes representing the open borehole are assigned a permeability of 1×10^{-4} m^2, providing little resistance to flow in the open hole. The first onion skin in the upper 20 m of each hole are assigned a permeability of 5×10^{-19} m^2 and a diffusion coefficient (D*) of 5×10^{-19} m^2/s to simulate the effects of the steel casing. Nodes in the remaining onion skins are assigned the rock and tracer transport properties specified in a given simulation for the geologic unit in which they reside.

1.6. 3-D Simulations: Boundary and initial conditions

The domain was initialized with concentrations in the source region fixed to values representing the maximum observations and the two source regions were activated at the appropriate time from 1975 until 2006 (see Stauffer et al. [7] for a more thorough explanation of the plume generation algorithm). The initial concentration of TCA on a plane at a depth of 80 ft below the surface is shown on Figure 4. From this figure one can see the intersection of the plume with the atmosphere at the canyon slopes, where the plume delineates the narrow finger mesa on which MDA L is situated. The total width of the mesa at this location is only approximately 500 ft (152 m). The initial plume for the SVE simulations is slightly modified from Stauffer (2005) to account for more recent data in the vicinity of the extraction boreholes. Specifically, the concentrations in the East source region were lowered during the years 2004-2006 to better match data from boreholes BH-24243 and 54-2002. Additionally, the source locations in this higher resolution grid are modified slightly from Stauffer et al. [7], and the new simulation results for 2006 were compared to the data from the previous modeling combined with new data collected during 2004-2006. The model-data regression remained quite good with an r^2 correlation coefficient of greater than 0.89. Therefore we are confident that the initial condition for the 3-D SVE simulations is a very good representation of the actual plume beneath MDA L.

2. 3-D Model Calibration

2.1. Calibration goals

The goal of the calibration is not to find exact fits to all of the test data, but to find the set of parameters that will approximate the overall data trends. This is a vital point of the modeling study. Given the inherent uncertainty in the subsurface we will never be able to exactly match all of the data from the Pilot Test. We do, however, strive to recreate as many aspects of the test as possible given constrains on the number of simulations, the number of adjustable parameters (horizontal and vertical permeability), the spatial variability of parameters, and uncertainty in the applicability of representing the rock units in the mesa as single continua with average fracture/matrix properties. The two most robust data sets that we have for each test are the concentration versus time in the extraction stream and the pressure at the top of the wellbore. The primary calibration target is the extraction concentration, while the pressure at the top of the hole is fixed to the average value for both the East and West tests. A final calibration target is to

have the simulation maintain the approximate flow rate calculated from the data during the test period. Issues with pressure and concentration measurements in surrounding wellbores, discussed in Section 2.3.4, have led us to not use these data in the parameter estimation section of the calibration. However, we do discuss the relationship of these data to the results of the calibrated parameters.

2.2. Calibration details

Calibration of the 3-D model is performed using the AMALGAM parallel optimization algorithm of Vrugt et al. [37]. AMALGAM uses thousands of realizations to search the mulit-dimensional parameter space. AMALGAM is extremely adept at finding global minimum solutions. Observed VOC concentrations in the vapor phase at the tops of the East and West extraction holes during the initial 22-d pilot experiment were used for SVE model calibration. The basic idea is that we can determine the subsurface permeability distribution by matching the concentration versus time curve that is measured at the top of the extraction boreholes while simultaneously maintaining close agreement with measured borehole flow rates and pressure at the top of the borehole. For this scheme to work correctly, the initial state of the simulated plume must be fairly close to the in situ plume. The pre-SVE simulated plume versus data, as presented by a model-data correlation in Figure 7, shows that our initial state is fairly close to the data.

To ensure that the calibrated permeability distribution matches the data from the tests, we must impose several conditions on the simulations. The most restrictive calibration condition we use fixes the simulated pressure at the top of the extraction borehole to the average pressure measured during the test. The second calibration condition that we use is that the simulated flow rate at the top of the borehole must remain within 10% of the values calculated for each test shown in Table IV at all times after the first day. Simulations that fail either of these criteria are removed from the model calibration by giving the parameter value combination a large weighting term. The flow rate during the test was calculated from an equation provided by the manufacturer of the orifice plate used to measure the pressure drop across a slight decrease in the diameter of the extraction line. Table IV shows values for the average pressure drop across the orifice plate, wellhead pressure, wellhead suction, and calculated extraction rates for the Pilot Test. There are three distinct rates because the extraction vacuum was increased during the later part of the SVE West test. For the SVE West calibration, only the first 21.9 days were simulated so that we remained within the lower flow rate time period shown in Table IV.

Because the permeability data from the packer tests show wide variability within the subsurface at MDA L, the East and West SVE Pilot tests were calibrated separately. Figure 8 shows the relative locations of the SVE cased interval, the open borehole interval, and the rock units found at both the East and West SVE site. There are small differences in the rock thicknesses between the two sites, however these differences were not sufficient to allow one set of permeability values to calibrate both the East and the West tests. As calibration parameters, we selected the permeability of the rocks of the upper four geological units depicted in Figure 8. An initial sensitivity analysis demonstrated that deeper geological units had marginal impact on the simulation results. To simulate the effects of vertical cracks, separate values of the horizontal and vertical permeability were optimized for each rock type. We also optimized the permeability of asphalt because this material acts as an important diffusive barrier over almost the entire grid

surface. Permeability in the calibration was allowed to range from 1e-13 m2 to 1e-11 m2 to cover the ranges seen in the straddle packer data and core permeability measurements shown in Table III,

A distributed computing implementation of AMALGAM was used to optimize the SVE model parameters for the East and West pilot tests using a simple F_{SLS} objective function [38]. We used a population size of 10 points, and hence 10 different slave computers, in combination with 120 computing hours on the LISA cluster at the SARA parallel computing center (U of A, The Netherlands). Each of these nodes is equipped with a dual-core Intel® Xeon™ 3.4 GHz processor with 4 GB of memory. The optimization performed over 2000 realizations for both the SVE East and SVE West experiments. To reduce the complexity of the SVE West test, the data were compressed in time to remove the period during which the SVE system had failed (2.88-6.66 days). Additionally, some of the clearly spurious data outlier points were removed from the calibration target, providing a smoother version of the data curve than that which is presented in Figure 10.

Figures 10 and 11 present a time series plot of observed (solid circles) and simulated (solid line) VOC vapor phase outlet concentration at the western (Fig. 10) and eastern (Fig. 11) SVE extraction well. The corresponding optimized permeability values for the individual rock types are listed in Table V. In general, the fit to the observed data is quite good for both pilot tests after about 2 days, successfully capturing and simulating the process of matrix flow. However, during the first 2 days the SVE model significantly underestimates observed VOC concentrations. This initial misfit is probably caused by flow through joints and fractures, a process widely observed throughout the Pajarito Plateau and the experimental site, but not explicitly included in our model. We represent fracture flow by allowing AMALGAM to optimize the horizontal and vertical permeability in ranges above measured matrix values. This implementation combines the effect of matrix and fracture flow, and does not allow us to explicitly simulate flow through fractures, which would be required to match the early time data. Hence, much better predictions at the initial time steps are possible if we explicitly incorporate fracture flow in the model. One approach of doing this would be to augment the current SVE model with the generalized dual porosity model (GDPM) presented in Zyvoloski [37]. This method assumes one-dimensional transport into and out of the matrix using multiple closely-spaced nodes connected to the primary fracture nodes. This setup can capture preferential flow and transport processes and therefore will likely simulate the high initial extraction of VOC observed in the experimental data. We are currently in the process of including this in our SVE model as well. The results of this will be reported in a forthcoming paper.

The optimized permeabilities for the East and West pilot tests are in good agreement, generally within an order of magnitude difference. Such a spatial variability is observed in the field (Neeper [11]; Stauffer et al. [35]). Table V lists the values of permeability that were found to provide the optimal fits to the test data for both the East and West tests. SVE West required higher permeability in unit Qbt1-vu while SVE East required higher permeability in Qbt1-vc. Deeper units in both tests appeared to be better fit with values from the lower bounds of the packer data. Moreover, their optimized values are typically within the middle of the prior uncertainty ranges, only approaching the outer bounds for a few parameters. This finding increases confidence in our SVE model calibration, with parameter values that appear reasonable

and demonstrate the appropriate variability between locations. Despite this, given the presence of systematic errors in our model predictions, apparent during the first 2 days in both Fig. 10 and 11, over-conditioning to a single "best" parameter combination seems unjustified, and the assumptions underlying the classical approach to parameter estimation need to be revisited.

For all calibrations, the vertical and horizontal permeability of each rock unit shown in Table V was varied to find the best overall fit to the data as described above. Several simplifications have been made for the current calibration. Stauffer et al. (2007) gives a more detailed description of attempting to fit the rebound spike seen after the pump failure on the SVE West test; however for simplicity we have removed the restart interval from the current calibration exercise. We also run both the East and West tests out to only 21.9 days because this time interval contains the most useful data.

2.3. Calibration results

2.3.1. Top-hole pressure versus flow rate

The calibrated SVE West test has a top-hole pressure fixed at 66.8 kPa while the pressure at the top of the SVE East borehole is fixed at 63.4 kPa. Both East and West calibration runs were required to remain within 10% of the calculated extraction mass flow rates for all times after 1 day of simulation time. We only examine flow rate after one day of extraction, because the extraction rate in the simulations varies through time as the pressure wave moves through the rocks. The final flow rates in the calibration runs were both within the prescribed tolerance of 10% of the measured values. Figure 9 shows the simulated top-hole flow rate response for both the East and West tests compared to the average flow rate calculated from the Dwyer pressure plate equation for each of these tests. This plot shows that the flow rate reaches equilibrium during the extraction test within approximately one day.

2.3.2. Extraction concentration and total mass removal

Figure 10 compares the SVE West test data to the simulated concentration at the wellhead for the calibrated fit of the SVE West test. The single continuum is able to recreate the general trend of the extraction data. The early time simulation results do not show the initial rise in concentration that was observed, however the longer time trend of the simulation shows the same trailing behavior at about the same concentration that was seen in the test. The calibrated SVE East simulation versus data, shown in Figure 11, also does not capture the initial spike in concentrations seen in the data, but does capture the longer time tailing behavior at nearly the same concentration as seen in the data. Figure 12 shows that simulated total TCA mass removal versus time is a good fit to the data from both the SVE East test, however the flowrate for the West test was slightly higher than the flow rate calculated from the pressure plate data leading to a systematic over prediction of the total mass removed.

2.3.3. Concentrations in surrounding boreholes

Results from simulated concentrations in surrounding boreholes show that the model is capturing the magnitude and trend of the data (Figures 13, 14, and 15). Points in the model that were closest to the data were chosen for comparison; however because the grid spacing is 10 m in the x and y directions, the comparison points are somewhat offset. For example, BH-24240 is 3.5 m from the nearest model node, while 54-2002 is 6 m from the nearest grid node. Thus, we are not trying to determine exact fits between data and model. We are attempting to see if there is

agreement with the trend and magnitude of the data for the simulations at a point approximating the data location. Figure 13 shows simulated results versus data at a well (BH-24240) lying only 25 ft. laterally from the extraction borehole. This simulation uses the calibrated SVE W parameters run with more detailed logic including a well shut-in period to represent the broken pump interval. The simulation does not rebound, since we do not have dual continuum behavior, however the overall decline in concentration at the 50 ft. depth in borehole BH-24240 is a good match to the data. Figure 14 shows the decline in simulated concentration at a depth of 100 ft. in BH-24243, lying approximately 54 ft. from the SVE East extraction borehole. The simulated concentration change does not produce the sharp drop in concentration seen in the data, nor does the simulation lead to a large rebound after the SVE system is shut off. Because the data fall to near zero concentration so rapidly, the system is either extremely fracture dominated or there may be a problem with surface air being pulled down the sampling ports by the applied suction. The possibility of a problem with the sampling is discussed in more detail in Section 2.3.4. One of these two mechanisms must also be affecting the data from BH-2002 (Figure 15), located 130 ft. from the extraction hole. This borehole also shows a sharp drop in concentration to near zero in just a few days, with an equally rapid rise in concentration after the SVE system is shut off. It is very interesting to note that the simulated concentrations for the SVE East test track the data very well at both early and late times.

2.3.4. Pressure changes in surrounding boreholes

As with the surrounding concentration data, we pick a point that is most appropriate on the existing 3-D grid for the comparisons. For the manometer, because flow to the wellbore is fairly radial and there is no preexisting lateral pressure gradient in the mesa, we pick the node in the grid that is the closest in radial distance from the well. For this reason some of the manometer comparison points are not at the same node as the concentration comparisons for the same data points. For example, the closest node from the extraction borehole in the direction of the source region for BH-24240 is 16 ft., which was the node chosen for concentration comparison; however the node chosen for manometer comparison lies 27 ft. from the simulated extraction hole in a more westerly direction.

Figure 16 shows values for the calibrated simulation compared to manometer readings in ports located in boreholes 54-24240, 54-2002, and 54-24243. Interestingly, the data versus model correlation in borehole 54-24240 has one point where the data and model are in agreement; however in boreholes 54-24243 and 54-2002 the data show much lower pressure drops than the calibrated simulation. The simple, hand-held manometer readings are meant to be a qualitative tool; however the data collected may point to an underlying problem with the FLUTe^{TM} system (www.geoprobe.com/products/flute/flutedesc.htm, accessed on 7/2/2007) that otherwise would not have been noticed.

We now speculate on the possible causes for the differences between the manometer readings and the simulated subsurface pressure field. First, the hand-held manometers are hooked to tubes in the FLUTe^{TM} socks that line the sampling boreholes (Anderson et al., 2007). These socks may not be providing a complete seal, leading to manometer readings that are lower than that in situ pressure. One line of evidence that supports this conclusion is that the difference between the downhole pressure and the surface pressure while the extraction pump was shut down is very small, for most manometer readings the differences were less than 0.1 kPa even at depths of

greater than 100 ft. below the surface. Figure 17 shows that the magnitude of the barometric signal change during the time of the two tests can be as high as 1.6 kPa in only 2.5 days. Even in the absence of the SVE testing, barometric swings of this magnitude should lead to differences between the surface and the subsurface. Neeper [11] presents data collected from a borehole located 100 m to the East of the site that shows almost no pressure difference between the atmosphere and a port at 11 m depth. However at depths of 77 m and 103 m the amplitude of the pressure wave is depressed and phase shifted such that differences between atmospheric pressure and downhole pressure should vary between +0.6 and -0.6 kPa. Because differences between the downhole pressure and atmospheric pressure measured before and after the SVE tests were much smaller than this, and in many cases were virtually zero, we believe that there is a strong possibility that there is a pressure connection between the ports on the monitoring wells.

The possibility of ports leaking during the high suction of an SVE test raises the concerns that an incomplete seal on the sampling ports could lead to the high suction pulling fresh air down the sampling boreholes. Fresh air flowing down the sampling holes would lead to dramatic drops in concentration at all leaky depths, such as seen in the data for BH-24243 and BH-2002. Once the vacuum is removed, the ports would show rapid rebound. This may be a valid explanation for the extreme dual continuum behavior seen in the surrounding borehole concentration data. If this is indeed the case, the current model assumption of a single continuum may be more valid than we first thought.

2.3.5. Conclusions from the calibration

The general conclusions from the calibration are 1) that the upper unit near the SVE West test are more permeable than the upper units near the SVE East test and 2) that the bulk permeability on the West side is higher than on the East side. Furthermore, the fact that measured pressure changes at depth are not in agreement with previous pressure data point to possible problems associated with leaks in the sampling tubes. Such leaks would bring fresh air to depth, leading to sharp drops in apparent concentration that would quickly rebound after the suction is removed. The concentration data from boreholes surrounding the SVE East test particularly support this hypothesis over the dual continuum hypothesis because the extraction borehole concentrations do not show a corresponding drop in concentration to near zero, which one would expect to see if the concentrations in the incoming gas from nearby boreholes was truly at such low levels.

3. 3-D MODEL USED FOR DECISION ANALYSIS

One of the primary recommendations of the MDA L RFI report [34] was that a corrective measures study should be performed at this site. In this section we discuss how the results from the modeling can be used to guide decisions about possible remediation alternatives. Results from a hypothetical sudden release of VOC are presented to show how modeling can be used to explore scenarios that are relevant to demonstrating that SVE can be a successful corrective measure at MDA L.

The simulations presented in Section 3.1 are modified to explore how an SVE system can be used at MDA L to respond to catastrophic failure of drums containing VOC. We first estimate the time required to detect a catastrophic failure using the in-situ monitoring network and, by knowing how long it will take to detect such a failure suggest a sampling plan to maximize the 'early warning' capability of the monitoring network by showing which of the existing ports are

most useful for early detection. We envision that the early warning design can provide data for a decision point that can trigger activation of the SVE system if action levels are exceeded. Under this plan, the SVE system will not need to be run constantly, but will used as an auxiliary intervention device when needed. We next use the model to show the effectiveness of the SVE system to remediate any VOC released during such a hypothetical catastrophic event. The modeling shows that, even in extreme release scenarios for this site, SVE technology can be used successfully to extract the increased VOC load and stop any migration toward the regional water table. We must stress that 1) modeling is the only tool available to explore sudden failure, and 2) that the model results can be used in demonstrating to Stakeholders that the proposed closure plan is comprehensive and safe.

In Section 3.2, we discuss the results of a plume rebound analysis that is used to estimate the amount of time required for the plume to regenerate at the estimated pre-SVE leakage rate. Regeneration time is an important parameter in determining how often the SVE system may need to be utilized to ensure that the plume does not grow significantly.

3.1. Hypothetical sudden release scenario

In this section we present results from simulations of a sudden release of 3 and 5 drums of pure TCA in both the East and West source regions. We consider this amount to be at the upper end of a reasonable release because many of the drums at this site were filled with adsorbent material, and early releases were not containerized in drums.

The sudden release scenario simulations use the calibrated SVE parameters. These simulations are initiated with the pre-SVE plume in the year 2006; use the same fixed slow release in the source region from the best-fit calibration, and inject a pulse of TCA beneath the shafts to represent the drum failures. Using the TA-21 diesel leak as a guide, we assume that the release as liquid reaches depths between 60 ft to 120 ft. As seen on Figure 8, the hypothetical sudden release reaches from the middle of unit Qbt 1v-u into the top of unit Qbt 1v-c. The vapor phase concentration of the release is fixed at the vapor pressure limit of TCA (160,000 ppmv) for varying amounts of time to generate 3 drums (843 kg TCA) and 5 drums (1405 kg TCA) in both the East and West source regions. For example, simulation of a three drum failure using this conceptual model requires that the region below the shafts be fixed for 8.12 days while the 5 drum case requires 86.25 days of fixed concentrations to generate the required mass in the release area. The location of the sudden releases on the east and west sides of MDA L are shown on Figure 18. One primary assumption in this release scenario is that once the liquid flows to the prescribed depth, it quickly volatilizes and the resulting vapor plume grows only through diffusion away from high concentrations in the release area.

This simplified release scenario does not take into consideration the density change caused by 160,000 ppmv TCA in the pore gas. Gas containing this concentration of TCA would be about 1.6 times denser than the rest of the pore gas in the mesa, and could lead to advective transport to greater depths. This underscores the importance of quickly identifying such a release and having a rapid response plan that can be quickly implemented.

3.1.1. Plume growth due to sudden release detected in surrounding boreholes

After the mass representing the release of drums is input to the model, the simulation is continued for 5 years to provide insight into how fast such a plume may be detected in surrounding sentry wells. Figure 19 shows the 5 year response in several surrounding boreholes at a depth of 150 ft. to a sudden release of 5 drums beneath both the East and West source regions. This figure shows that the concentrations rise dramatically after only one year in the boreholes closest to the sudden release. Borehole C (54-24240) and BH-I (not yet constructed) are both located 14 m (46 ft.) from the hypothetical release and show very similar behavior. Concentrations rise from less than 500 ppmv to greater than 2000 ppmv in the first year, with continued increases until the plume begins to diffuse away after 2 years. For borehole H (54-24243), located 22.2 m (73 ft.) from the hypothetical release, the response is muted; however concentrations rise from 270 ppmv to over 700 ppmv in the first year and continue to rise. The response for the 3 drum scenario is shown in Figure 20 and has the same character as the 5 drum scenario but lower total increases for each of the sentry wells. Boreholes E (54-24238) and F (54-24243), located 93 ft. and 98 ft. respectively from the release area show similar behavior (Figure 21) and suggest that wells located within 100 ft. of any significant release (3-5 drums) should provide timely evidence of such a release. Wells that could be used for sentry wells include boreholes 54-24243, 24240, 24238, and the soon to be completed boreholes H, I, and J. Because the nearby simulations showed a robust response to the sudden release at all depths between 25 ft. and 150 ft., only one or two ports from each of these wells should be sampled quarterly. If sudden increases in concentration at the sentry ports are detected, we recommend sampling all ports at that location to see if the increase is affecting the entire depth interval. Once it is determined that an increased release is occurring, there should be metrics in place to determine when to initiate the SVE system. One possibility would be to have a target concentration, such as 1000 ppmv at which time the release is considered significant enough to turn on the SVE system. Another approach would be to compare several quarters of data before the sentry ports began increasing in concentration and make the action level be a function of the pre-increased leak. For example, action could be triggered if ports at given sentry well increase in concentration by a factor of 2 or 3 times their long term near steady values, and the SVE system turned on to remediate the increased leak.

3.1.2. Effectiveness of remediation on the hypothetical 5 drum sudden release

We next present results from a hypothetical SVE operation on the 5 drum release described above. Because of the similarity of the results for the 3 and 5 drum scenarios, for the rest of the report we discuss only the 5 drum case. For this simulation we assume that the site operators have determined that a release has occurred and implemented a corrective measure one year after a sudden release of 5 drums. Simulations were done simultaneously for both the East and West release areas. Figure 22 shows the plume just prior to the beginning of the SVE operation, after one year of plume growth from the 5 drum scenario, on a slice plane approximately 80 ft. below the mesa top. Concentrations in the center of the source release areas remain quite high, and the 1000 ppmv contour has moved outward significantly from the source region as can be seen by comparing this figure to the plume shown in Figure 4. After one year of SVE pulling 0.049 kg/s from the SVE West borehole and 0.052 kg/s from the SVE East borehole, the extraction was stopped and the plume was allowed to rebound for one year.

Figure 23 shows the concentration versus depth profile beneath the western release area for the series of events beginning with the pre-sudden release 2006 plume, followed by one year of plume growth from the 5 drum failure scenario, followed by one year of SVE, and an additional year of plume rebound. During the entire simulation the original pre-sudden release source region continues to release TCA at the same rate as before the release. Concentrations after 1 year of plume growth are quite high in the upper 200 ft. while at greater depths concentrations are close to the 2006 pre-sudden release plume. After one year of SVE extraction, concentrations in the upper 130 ft. have been reduced to below the pre-sudden release plume values; however below this depth the concentrations remain higher than the pre-sudden release plume. Higher concentrations at depth after one year of SVE are due to the lower permeabilities used in the simulations for the Qbt 1g unit. Because our assumed sudden release scenario may underestimate the vertical migration of TCA, it may be necessary to modify the current SVE system to more efficiently remove VOC from unit Qbt 1g and below. One possible technique would be to retool the current SVE boreholes to include packers that could isolate suction on the lower portions of the borehole. This approach could be costly due to the complex technology needed. Other drawbacks include the necessity to use a smaller diameter inner casing to allow sections to be isolated, and also the fact that the current holes only goes to 215 ft. deep. The second approach would be to drill two new SVE boreholes, located directly next to the current SVE boreholes. These holes could be drilled to 300 ft. and cased to the 150 ft. level, allowing more efficient removal of VOC from this depth range. The co-location of the pairs of SVE holes would allow the SVE system to quick switch between depth intervals by simply moving the hose from the top of one hole to the top of the other hole.

The final part of the 5 drum SVE extraction simulation shown on Figure 23 involves one year of plume rebound from the slowly leaking source region the upper 60 ft., after which time the concentrations in the upper 60 ft. are back to the original pre-SVE values. Concentrations in the Qbt 1g unit are beginning to decrease as diffusion spreads the plume both laterally and vertically.

Figure 24 shows concentrations beneath the eastern sudden release area for the same series of events. Concentrations at the release area do not drop as significantly in the upper 130 ft. because the SVE East borehole is located further from the source. Concentrations in the upper 60 ft. rebound to values higher than the 2006 plume because the leak rate applied was based on the year 2000 plume generation which has slightly higher concentrations in the source region than the year 2006 pre-SVE plume; this slight difference does not affect the conclusions.

3.1.3. No further action

Figure 25 shows concentration beneath the western sudden release area at various times over the span of 100 years starting from the 5 drum sudden release scenario. The final curve shown on Figure 24 has no sudden release and only includes the effects of continued slow release for 100 years. Note that the sudden release includes continued slow release after the initial release, so that the difference in total mass input for the final two curves on Figure 24 is only 5 drums (1405 kg) of TCA. These two cases are the 'No Further Action' cases and show that although early time concentrations from a 5 drum release lead to significant increases in concentrations in the upper 200 ft. of the mesa, the long term diffusive nature of the plume will tend to smear the sudden release such that after 100 years there is little difference between continued slow release and the sudden release. After one year the 100 ppmv contour has reached the bottom of unit Qbt

1g. By 20 years, this contour has dropped to the middle of the Otowi member of the Bandelier Tuff. Within 50 years the 100 ppmv contour is at the top of the Tb4 Basalt.

Figure 26 expands the depth of Figure 25 and includes the regional aquifer depth. At no time in the 100 year simulations, either with or without the sudden release of 5 drums, does the 10 ppmv contour drop below 650 ft. below the top of the mesa. At 800 ft. below the mesa to, concentrations are below 3 ppmv, suggesting that releases from this site, including both sudden releases and slow leaks, will not impact the regional aquifer located at approximately 950 ft. below the mesa top.

3.2. Plume rebound after one year of SVE

Finally, we present a simulation showing how the total mass of the plume may rebound after one year of SVE. Figure 27A shows the total mass in the plume as a function of time. During the first year of the simulation, both the East and West SVE boreholes have pressures fixed at 64.3 and 66.8 kPa respectively. During the entire simulation, VOC is allowed to leak at the pre-SVE leakage rate from both source regions. During the extraction (Figure 26B), the plume loses more than 40% of its mass during the first three months of SVE. After 3 months of extraction, the rate of withdraw decreases significantly, showing that the most efficient timeframe to run the SVE system is on the order of 2-3 months.

After the SVE system is shut down, the plume begins to grow slowly at the pre-SVE leakage rate. As seen on Figure 27A, the plume does not rebound to its original size after 9 years of growth from the imposed slow leaks. This implies that in the absence of a catastrophic drum failure, activation of the SVE system every few years should be sufficient to control the continued growth of the plume. A best management practice solution to plume control at MDA L could be developed to maximize withdraw while minimizing the time required to run the SVE pumps and other equipment. Figure 27 suggests that such an analysis would likely result in a recommendation to run the SVE system for only 2 to 3 months every 1 to 3 years.

3.3. Radius of influence

The radius of influence for the simulated SVE West test is shown in Figures 28 A and B. The images are (A) a N-S slice and (B) an E-W slice through the SVE West site. The purple colored region in both images is below the cut-off flux of 4.e-6 m/s. This cut-off flux translates to a true velocity of about 0.7 m/day or 41 m in 60 days. The region of active extraction is limited to the higher permeability rocks. The radius of influence is not symmetric with respect to the mesa and is influenced by the geometry and permeability structure of the mesa.

4. CONCLUSIONS

Data collected during a one month SVE test are sufficient to calibrate a site-scale 3-D model of VOC transport at MDA L. Some questions developed during the calibration of the manometer data suggest that the FLUTe^{TM} system in surrounding boreholes may be leaking, especially during the high suction of the SVE test. This may in turn explain the extremely rapid drops in concentration at all depths in several of the monitoring wells. It would also explain the manometer readings taken before and after the SVE test that show almost no differential pressure between the surface and ports at a range of depths to 200 ft.

Simulations of a sudden release of VOC show that the current and planned monitoring holes within 100 ft. of the source regions at MDA L will be useful sentry wells. We recommend that one or two ports from these wells be sampled every quarter and examined for sudden increases in concentrations. If such increases are seen, the rest of the ports in the affected well should be sampled and trend analysis performed over the span of a few quarters. Additionally, action criterion should be developed to determine at what level of increased concentrations a significant leak has occurred. The action levels should trigger the activation of the SVE system to promptly remediate a sudden release. Prompt action will limit the time that any sudden release will have to migrate to depth. The SVE system should be run until extracted concentrations drop below some target level, such as 100 ppmv (4.6e5 ug/m3).

Simulation of SVE extraction after a release of 5 drums of VOC shows that the current system can remove a significant portion of the release. Concentrations in the upper 130 ft. of the mesa were reduced through time by SVE pumping to levels well below the pre-sudden release; however concentrations below this depth were not as efficiently removed from the mesa. The presence of higher permeability rocks in the more shallow sections of the mesa means that the SVE system preferentially pulls contaminants from the 0 – 130 ft depth interval. In the event that density driven transport of vapor phase VOC reaches depths greater than presented in our simplified release scenario, we recommend installation of two additional boreholes that would be drilled to 300 ft. and isolate the lower 150 ft. of the borehole. This system would allow removal of contaminants to the top of the Otowi unit and provide and extra level of safety in the event of a sudden release. Simulations of the 'No Further Action' option for both sudden releases and long term slow leaking at estimated current rates show that the plume is unlikely to reach the regional aquifer at concentrations greater than a few ppmv in the next 100 years. This result shows that the ability of the mesa to diffuse VOC is quite impressive.

Calculations of plume rebound show that in the absence of a catastrophic drum failure, activation of the SVE system every few years should be sufficient to control the continued growth of the plume. Finally, the radius of influence in the more permeable units is on the order of 40 m when for the SVE West test.

5. REFERENCES

1. W.A. JURY, D. RUSSO, G. STREILE, and H. ABD, "Evaluation of Volatilization by Organic Chemicals Residing Below the Soil Surface", Water Resour. Res. 26:13-20 (1990).

2. C.W. FETTER, Contaminant Hydrogeology, Prentice-Hall, NJ, USA (1999).

3. J.H. Lehr, Wiley's Remediation Technologies Handbook, Major Contaminant Chemicals and Chemical Groups, John Wiley and Sons, Hoboken NJ (2004).
4. S. HOEG, H.F. SCHOLER, and J. WARANTZ, "Assessment of interfacial mass transfer in water-unsaturated soils during vapor extraction", J. of Contaminant Hydrology 74:163-195 (2004).
5. G.C. BRADNER and L.C. MURDOCH, "Effects of skin and hydraulic fractures on SVE wells", J. of Contaminant Hydrology 774:271-297 (2005).

6. K. PREUSS and J.S.Y. WANG, "Numerical Modeling of Isothermal and Nonisothermal Flow in Unsaturated Fractured Rock: A Review", in Flow and Transport Through Unsaturated Fractured Rock, Second Edition, Geophysical Monograph 42, eds. D.D. EVANS, T.J. NICHOLSON, and T.C. RASMUSSEN, AGU, Washington D.C. (2001).
7. P.H. STAUFFER, K.H. BIRDSELL, M.S. WITKOWSKI, and J. K. HOPKINS, "Vadose Zone Transport of 1,1,1-Trichloroethane: Conceptual Model Validation through Numerical Simulation", Vadose Zone Journal 4(3): 760-773 (2005).
8. T. ANDERSON, "A Soil Vapor Extraction Pilot Study in a Deep Arid Vadose Zone, Part I", WM Symposium Proceedings, this volume (2007).
9. BROXTON D.E., and D.T. VANIMAN, "Geologic Framework of a Groundwater System on the Margin of a Rift Basin, Pajarito Plateau, North-Central New Mexico", Vadose Zone Journal 4(3):522:550 (2005).
10. D.A. NEEPER and R.H. GILKESON, "The influence of Topography, Stratigraphy, and Barometric Venting on the Hydrology of Unsaturated Bandelier Tuff", New Mexico Geological Society Guidebook, 47th Field Conference, Jemez Mountains Region, pp. 427-43 (1996).
11. D.A. NEEPER, "Investigation of the vadose zone using barometric pressure cycles", J. of Contaminant Hydrology 54, 59–80 (2002).
12. A.D. LITTLE, "The Installation Restoration Program Toxicology Guide", 1:1–16 (1987).
13. S.K. ONG and L.W. LIONS, "Effects of soil properties and moisture on the sorption of trichloroethylene vapor", Water Res. 25: 29–36 (1991).
14. R. SANDER, "Henry's Law Constants" in NIST Chemistry WebBook, NIST Standard Reference Database Number 69, P.J. LINSTROM and W.G. MALLARD (ed.), National Institute of Standards and Technology, Gaithersburg MD (2003).
15. H.R. FUENTES, W.L. POLZER, and J. L. SMITH. "Laboratory Measurements of Diffusion Coefficients for Trichloroethylene and Orthoxylene in Undisturbed Tuff", J. Environ. Quality, 20:215-221 (1991).
16. E.P. SPRINGER, "Statistical Exploration of Matrix Hydrologic Properties for the Bandelier Tuff, Los Alamos, New Mexico", Vadose Zone Journal 4:505-521 (2005).
17. K.H. BIRDSELL, A.V. WOLFSBERG, D. HOLLIS, T.A. CHERRY, and K.M. BOWER, "Groundwater Flow and Radionuclide Transport Calculations for a Performance Assessment of a Low- Level Waste Site", J. of Contaminant Hydrology 46:99-129 (2000).
18. D.B. ROGERS and B.M. GALLAHER, "The unsaturated characteristics of the Bandelier Tuff", Los Alamos National Laboratory Report, LA-12968-MS (1995).
19. B.A. ROBINSON, S.G. MCLIN, and H.S. VISWANATHAN, "Hydrologic Behavior of Unsaturated, Fractured Tuff: Interpretation and Modeling of a Wellbore Injection Test", Vadose Zone Journal 2005 4(3):694-707 (2005).
20. K.H. BIRDSELL, B.D. NEWMAN, B.A. ROBINSON and D.E. BROXTON, "Validation of the Conceptual Model for Vadose-Zone Flow and Transport beneath the Pajarito Plateau, Los Alamos, New Mexico", Vadose Zone Journal, 4:620-636 (2005).

21. G.A. ZYVOLOSKI, B.A. ROBINSON, Z.V. DASH, and L.L. TREASE, "Summary of the models and methods for the FEHM application-a finite-element heat-and mass-transfer code", Los Alamos National Laboratory report, LA-13307-MS (1997).

22. P.H. STAUFFER, L.H. AUER, and N.D. ROSENBERG, "Compressible gas in porous media: A finite amplitude analysis of natural convection", Int. J. of Heat and Mass Transfer, 40 (7), 1585-1589 (1997).

23. P.H. STAUFFER and N.D. ROSENBERG, "Vapor phase transport at a hillside landfill", Environmental and Engineering Geoscience, Vol. VI, No. 1, p. 71-84 (2000).

24. A.V. WOLFSBERG and P.H. STAUFFER, "Vadose-zone fluid and solute flux: advection and diffusion at the Area 5 Radioactive Waste Management Site", Los Alamos National Laboratory Report, LA-UR-03-4819 (2004).

25. D.A. NEEPER and P.H. STAUFFER, "Unidirectional gas flow in soil porosity resulting from barometric pressure cycles", J. of Contaminant Hydrology, 78(4), 281-289 (2005).

26. E.M. KWICKLIS, A.V. WOLFSBERG, P.H. STAUFFER, M.A. WALVROORD, and M.J. SULLY, "Multiphase Multicomponent Parameter Estimation for Liquid and Vapor Fluxes in Deep Arid Systems Using Hydrologic Data and Natural Environmental Traces", Vadose Zone Journal, 5:934-950 (2006).

27. P.H. STAUFFER, "Flux Flummoxed: A Proposal for Consistent Usage", Ground Water, 44(2): 125-128 (2006).

28. R.H. BROOKS and A.T. COREY, "Properties of porous media affecting fluid flow", Proceedings, American Society of Civil Engineers, Irrigation and Drainage Division 92(IR2):61-87 (1966).

29. C.S. FEN and L.M. ABRIOLA, "A comparison of mathematical formulations for organic vapor transport in porous media", Advances in Water Resources, 27:1005-1016 (2004).

30. D. RODRIGUEZ, "Significance of Diffused Zone Mass Flux Plumes in Determining the Longevity of Solute Plumes Emanating From Heterogeneous DNAPL Source Zone" Ph.D. Dissertation , Colorado School of Mines (2006).

31. T.D. GIDDA, D. CANN, W.H. STIVER, and R.G. ZYTNER, "Airflow dispersion in unsaturated soil", J. Contaminant Hydrology, 82(1), 118-132 (2006).

32. R.J. PAWAR and G.A. ZYVOLOSKI, "A Novel Method to Couple Wellbore Flow to Reservoir Flow", in Proceedings of the XVI International Conference on Computational Methods in Water Resources, edited by P.J. BINNING, P.K. ENGESGAARD, H.K. DAHLE, G.F. PINDER and W.G. GRAY, Copenhagen, Denmark, June, (2006).

33. J. HUANG and N.G. GOLTZ, "Solutions to equations incorporating the effect of rate-limited contaminant mass transfer on vadose zone remediation by soil vapor extraction", Water Resources Research 35(3):879-883 (1999).

34. LANL, "RCRA Facility Investigation Report, Los Alamos National Laboratory, Material Disposal Area L at Technical Area 54", LANL publication LA-UR 02-7803 (2003).

35. Stauffer, P.H., J.K,. Hopkins, and T. Anderson, "A Soil Vapor Extraction Pilot Study in a Deep Arid Vadose Zone Part 2: Simulations in Support of Decision Making Processes", Waste Management Conference proceedings paper, Tucson AZ, Feb 26-March 1 2007.

36. Vrugt, J.A., B.A. Robinson and M. Hyman, 2007 (in review). "A Universal Multimethod search strategy for computationally efficient global optimization" IEEE Transactions on Evolutionary Computation.

37. Zyvoloski, G. (2007 submitted) "FEHM: A control volume finite element code for simulating subsurface multi-phase multi-fluid heat and mass transfer", Vadose Zone Journal.

38 Vrugt, J.A., P.H. Stauffer, Th. Wohling, B.A. Robinson, and V.Vesselinov, (2007 in review) "Inver Modeling of Subsurface Flow and Transport Properties Using Recent Advances in Global Optimization, Parallel Computing and Sequential Data Assimilation" Vadose Zone Journal.

Table I 1,1,1-TCA Physiochemical Parameters

1,1,1-TCA ($C_2H_3CL_3$)	
Molecular weight [12]	133 g/mol
Liquid density [12]	1325 kg/m3 (at 293 K)
Vapor pressure [12]	100 mmHg (at 293 K)
Water solubility (mg/l) [12]	950 mg/L (at 293 K)
Tuff sorption coefficient K_d [13]	< 0.08 mL/kg fully saturated
Henry's Law constant (H_{TCA}) [14]	62 MPa/(liquid mole fraction) equal to 0.458 $(g/L)_{vapor}/(g/L)_{liquid}$ (at 285 K)
Diffusion coefficient in crushed Bandelier tuff assumed to be nearly equal to TCE $J = -\theta_a D \text{ grad}C$ where J is flux, θ_a is volumetric air content, C is the concentration, and D is the diffusion coefficient. [15]	4.6 e-6 to 9.3 e-6 m^2/s at 2-7% relative saturation 4.4e-7 to 1.4e-6 m^2/s at 29-36% relative saturation

Table II Porosity, saturation, and effective diffusion coefficient values used in the simulations.

Unit	Effective porosity	In-situ saturation	D* (m^2/s)
Qbt 2	0.41[a]	0.06[b]	$3x10^{-6}$
Qbt 1vu	0.49[a]	0.15[b]	$2x10^{-6}$
Qbt 1vc	0.49[a]	0.15[b]	$2x10^{-6}$
Qbt 1g	0.46[a]	0.15[b]	$2x10^{-6}$
Cerro Toledo (Qct or CT)	0.45[a]	0.40[b]	$5x10^{-7}$
Otowi Member (Qbo)	0.44[a]	0.35[b]	$5x10^{-7}$
Cerros del Rio basalt	0.1[b]	0.02[c]	$3x10^{-6}$
Land surface	0.48[c]	0.02[c]	$3x10^{-6}$
Asphalt	0.5[c]	0.02[c]	$1x10^{-14}$
Shafts	0.5[c]	0.02[c]	$3x10^{-6}$
Wellbore	1.0	0.001	$3x10^{-6}$
Well Casing	0.5	0.001	$1x10^{-14}$

[a] fixed to mean measured value from Springer [16]
[b] fixed to measured values reported in Birdsell et al. [17]
[c] assigned fixed value for the simulations

Table III In situ and core permeabilty data for the MDA L area.

GeologicUnit	0.6 m Packer Permeability (m^2) Includes fractures [18]			Mean Core Permeability (m^2) Matrix only [16]
	MIN	MEAN	MAX	
Qbt 2	5.3e-13	1.7e-12	3.8e-12	2.0e-13
Qbt 1vu	4.7e-13	2.9e-12	1.6e-11	1.2e-13
Qbt 1vc	8.5e-14	1.5e-12	1.2e-11	1.2e-13
Qbt 1g	1.1e-13	2.5e-12	5.4e-11	1.3e-13
Qtt (TT)	9.3e-13	7.5e-12	1.7e-11	NA
Qct (CT)	1.2e-12	5.7e-12	1.1e-11	NA
Qbo	5.5e-13	6.1e-13	7.1e-13	2.3e-13[b]

[b] Canada del Buey data

Table IV Extraction pressure and flow calibration targets for the SVE Pilot Tests

Test period	Average pressure drop across orifice plate (inches of water)	Pressure at the top of the wellhead[a] (kPa)	Wellhead suction (inches of Hg)	Calculated mass flow rate (kg/s)	Calculated volumetric flow rate (standard ft^3/min[b])
SVE West 0 - 21.9 days	3.66	66.8	3.9	0.0487	85.61
SVE West 21.9 – 28.7 days	4.68	65.1	4.4	0.0543	95.45
SVE East	4.46	63.4	4.9	0.0523	91.97

[a] assumes constant atmospheric pressure of 80kPa at the wellhead
[b] standard cubic feet per minute assumes air at a density of 1.206 kg/m3

Table V Calibrated permeabilities in both the horizontal and vertical directions used for the SVE Pilot Test simulations (Results from AMALGAM Calibration).

Unit	SVE West permeability m^2		SVE East permeability m^2	
	x , y	z	x , y	z
Qbt 2	6.5e-13	4.6e-13	1.0e-13	1.0e-13
Qbt 1vu	6.0e-12	2.0e-12	3.5e-12	1.6e-12
Qbt 1vc	1.0e-13	5.7e-13	8.4e-13	6.0e-12
Qbt 1g	1.0e-13	5.1e-13	1.0e-13	1.0e-13
Qtt (TT)	5.0e-13	5.0e-13	5.0e-13	5.0e-13
Qct (CT)	5.0e-13	5.0e-13	5.0e-13	5.0e-13
Qbo	1.5e-13	1.5e-13	1.5e-13	1.5e-13
Asphalt	1.9e-13	1.9e-13	1.0e-11	1.0e-11
Wellbore	1.0e-4	1.0e-4	1.0e-4	1.0e-4
Well Casing	5.0e-19	5.0e-19	5.0e-19	5.0e-19

Table VI Surrounding Borehole Manometer Data compared to Simulated Pressure Response for Selected Monitoring Ports

Borehole	Monitoring port depth (ft)	Pressure change from initial condition (-ve kPa)	
		Data	Model
24240	25	0.2	0.67
	50	0.6	1.31
	75	1.8	1.88
	100	1.5	2.34
	125	1.0	2.97
	150	0.5	2.87
24243	25	0.1	1.22
	50	0.1	2.32
	75	0.2	2.53
	100	0.7	2.70
	117	0.8	2.79
2002	60	0.1	1.38
	100	0.25	1.45
	140	0.27	1.41
	200	0.4	1.15

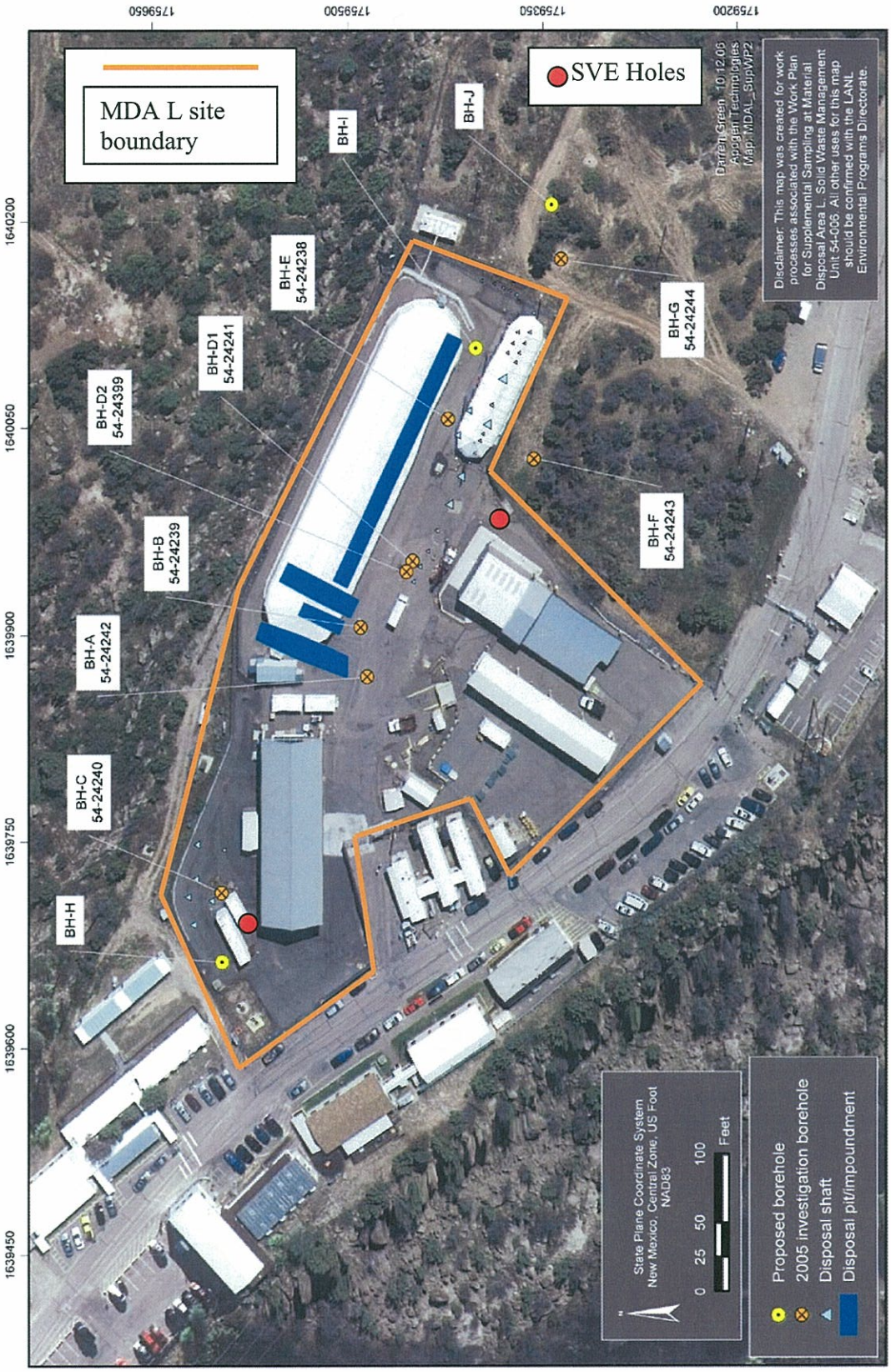

Figure 1: MDA L Site Boundary, monitoring boreholes, and SVE locations.

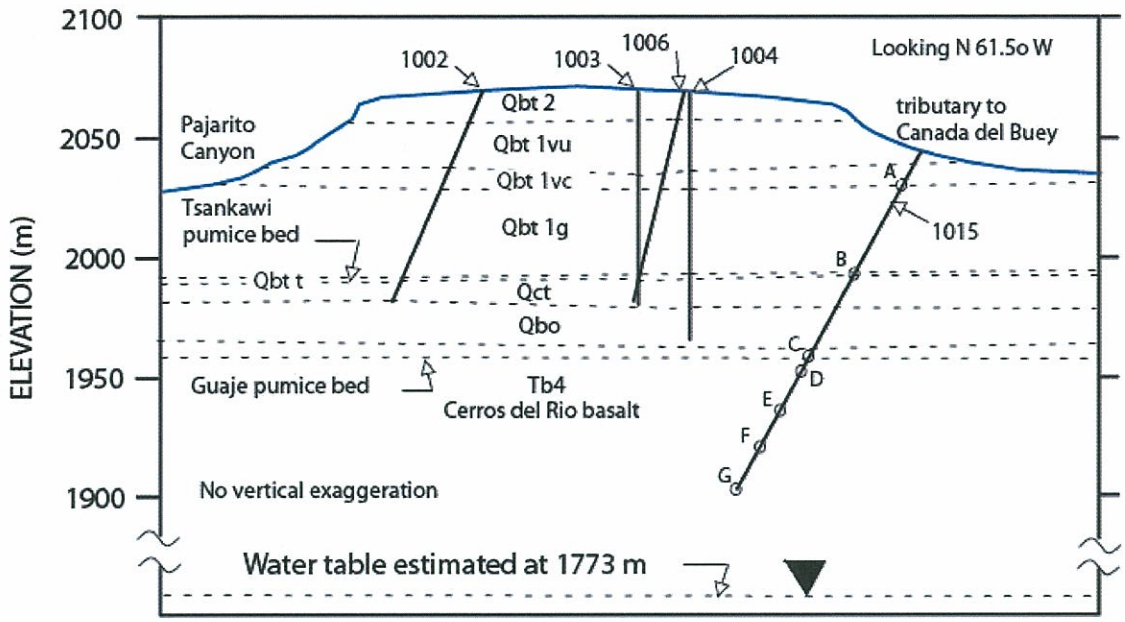

Figure 2 Site stratigraphy with wells lying immediately to the east of MDAL, After Neeper 2002.

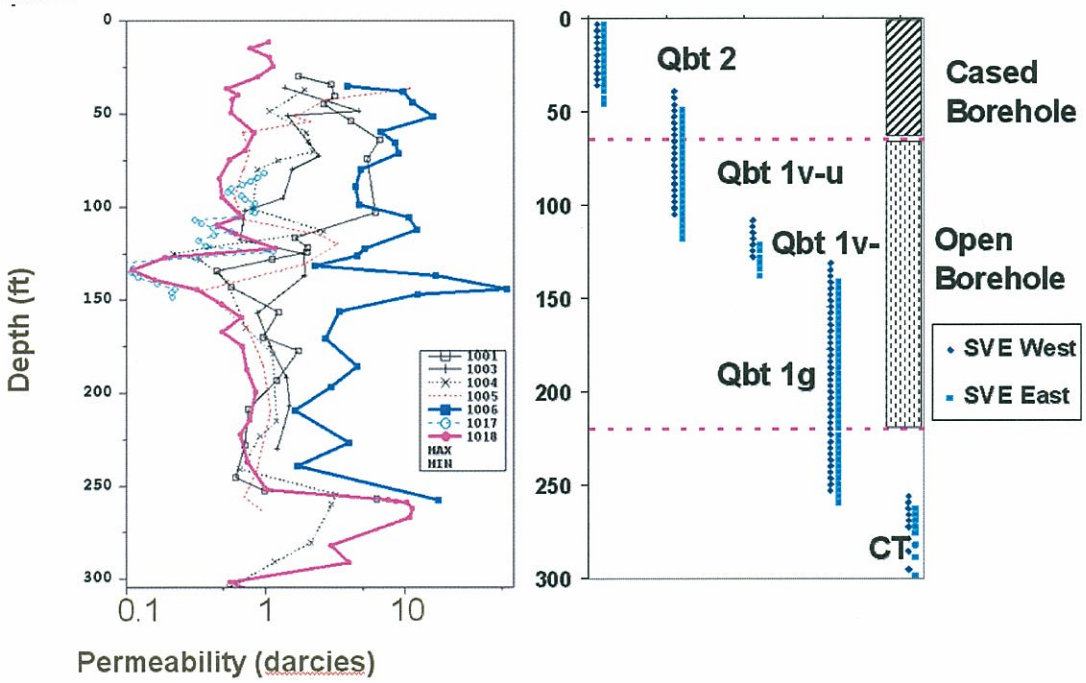

Figure 3 Straddle packer permeability data related to geologic units and the SVE borehole design.

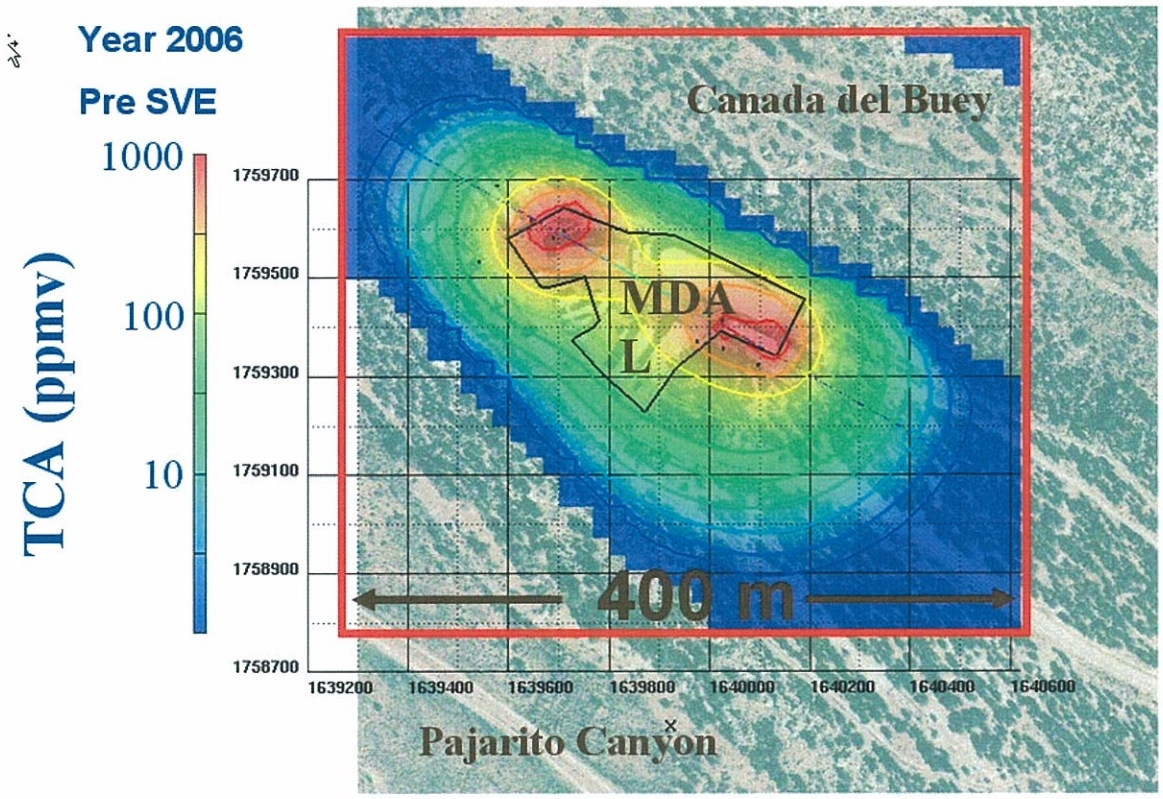

Figure 4 The lateral extent of the numerical grid is shown by the red line. Contours show a simulated concentration profile of the pre-SVE plume on a plane 80 ft. below the mesa top. The aerial photograph shows the relationship of the site boundary to Pajarito Canyon and Pajarito Rd. which runs through the text for Pajarito Canyon.

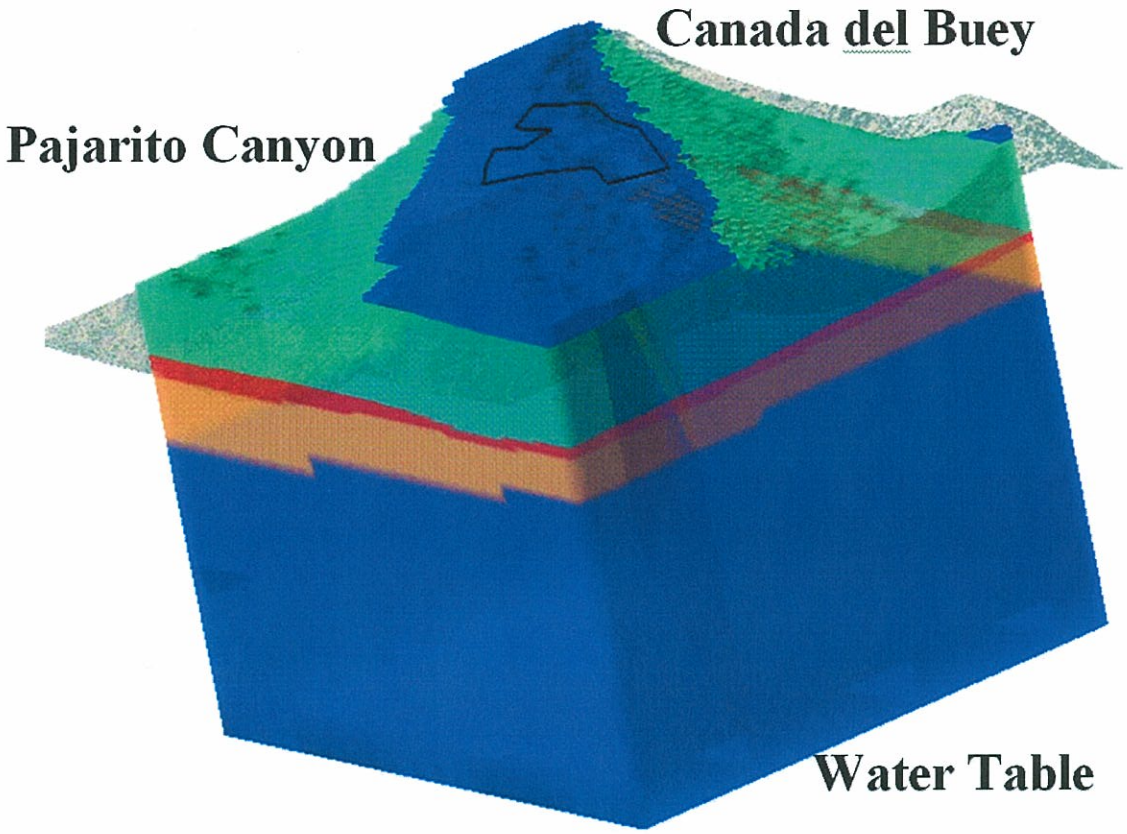

Figure 5 Angled view of the numerical grid with gross stratigraphy and MDA L outline. The topography of the grid is apparent from the way the model surface follows the aerial photograph that has been draped onto the digital elevation model of the site.

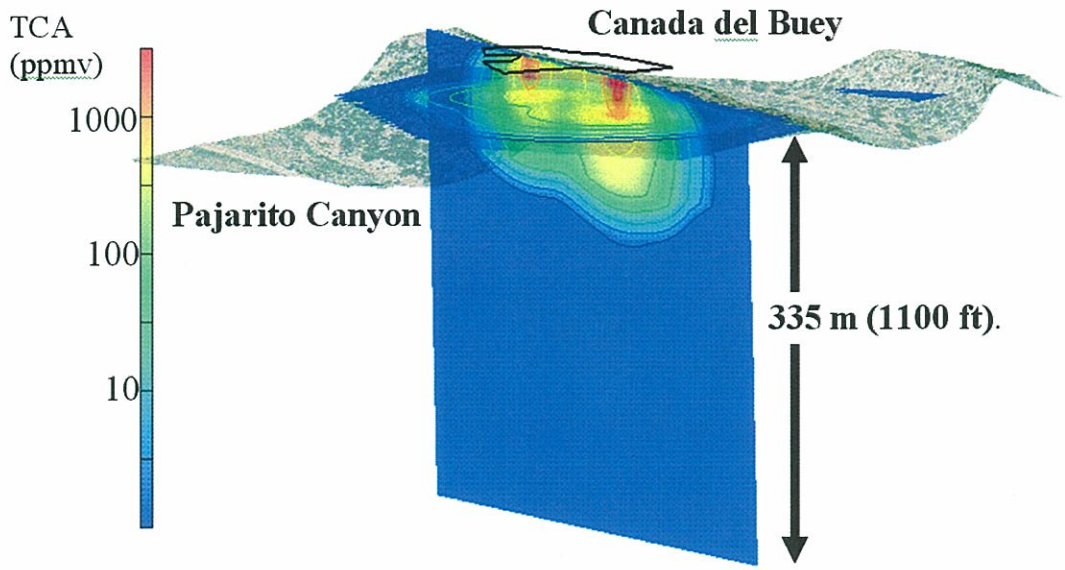

Figure 6 Slice planes of the numerical grid with concentration contours in ppmv showing the simulated pre-SVE Pilot test plume. The aerial photograph is draped onto the digital elevation model of the site and shows the canyons on either side of the mesa. The MDA L site boundary is the black polygon lying above the aerial photograph.

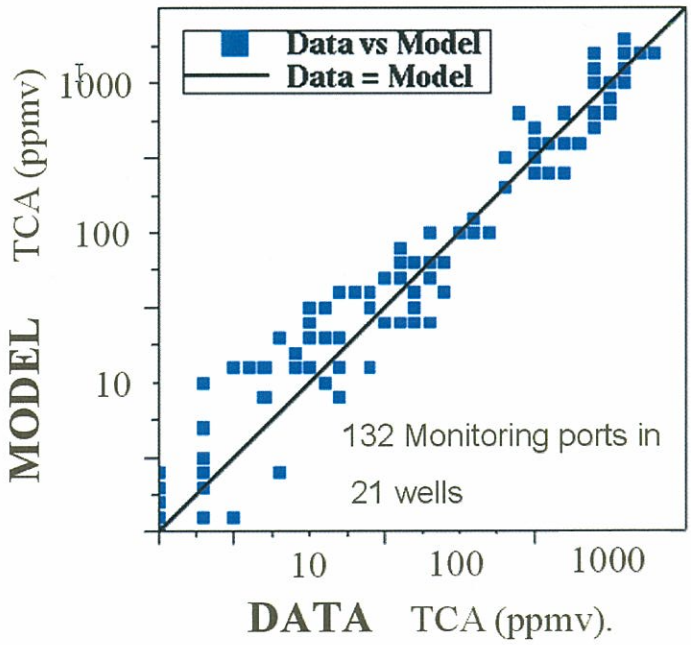

Figure 7 Model data regression for the pre-SVE Pilot Test simulated plume.

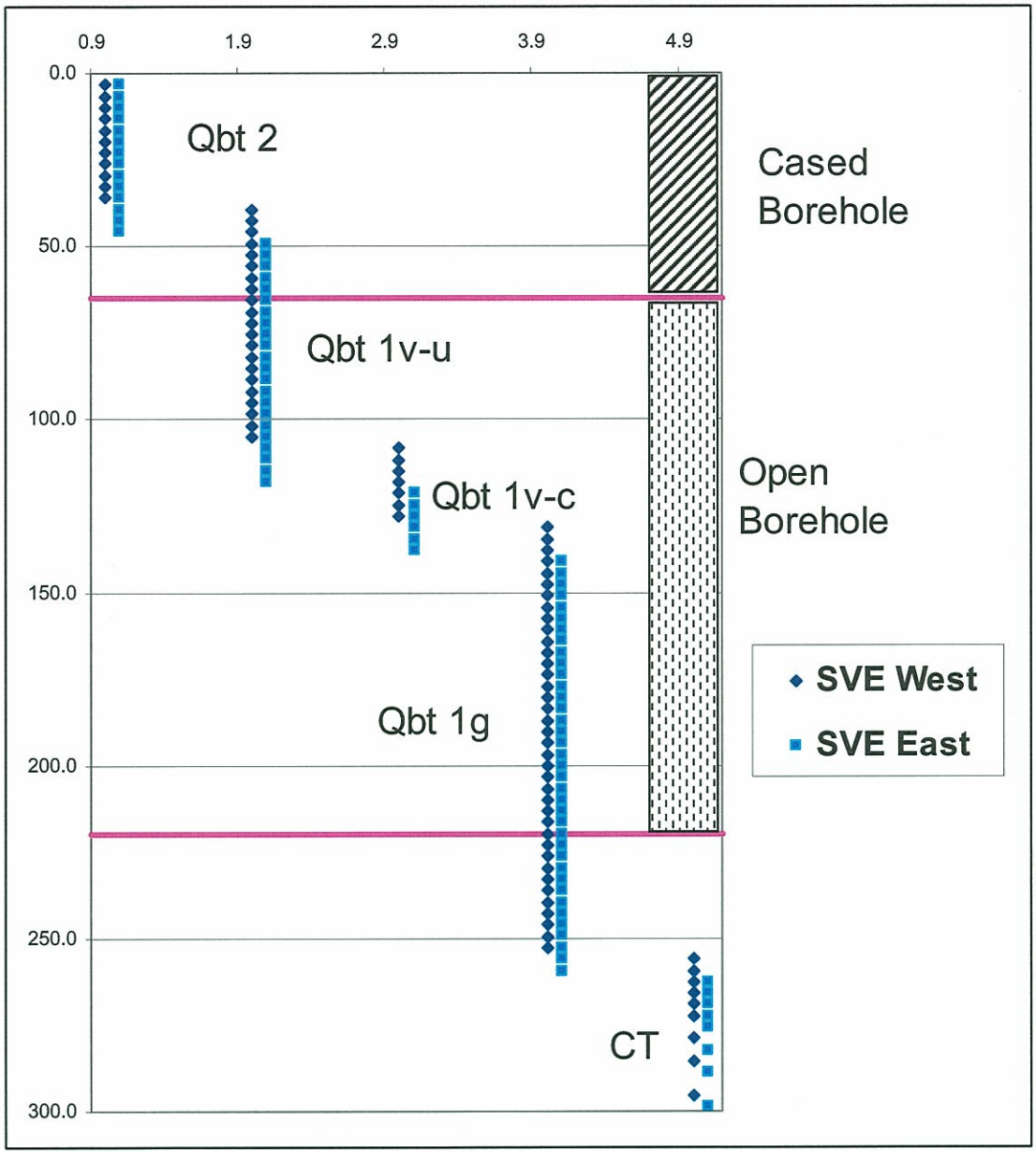

Figure 8 Site stratigraphy for the SVE boreholes in relationship to the well construction.

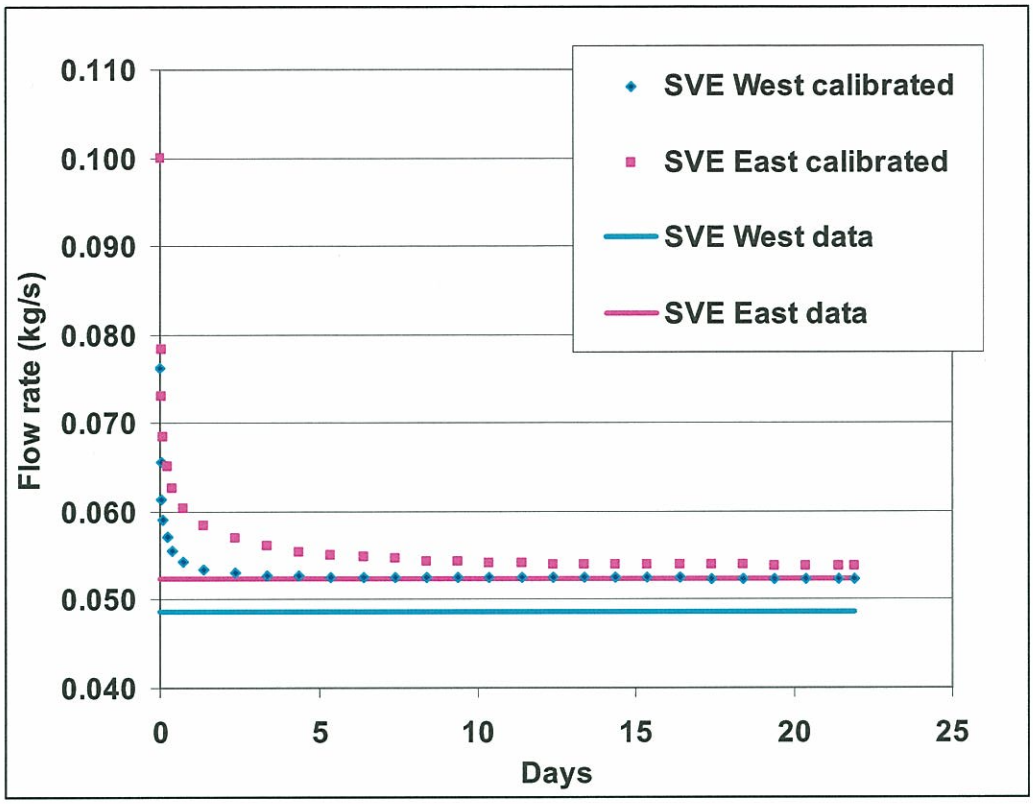

Figure 9 Simulated flow rates in the extraction boreholes compared to calculated flow rates for the East and West tests.

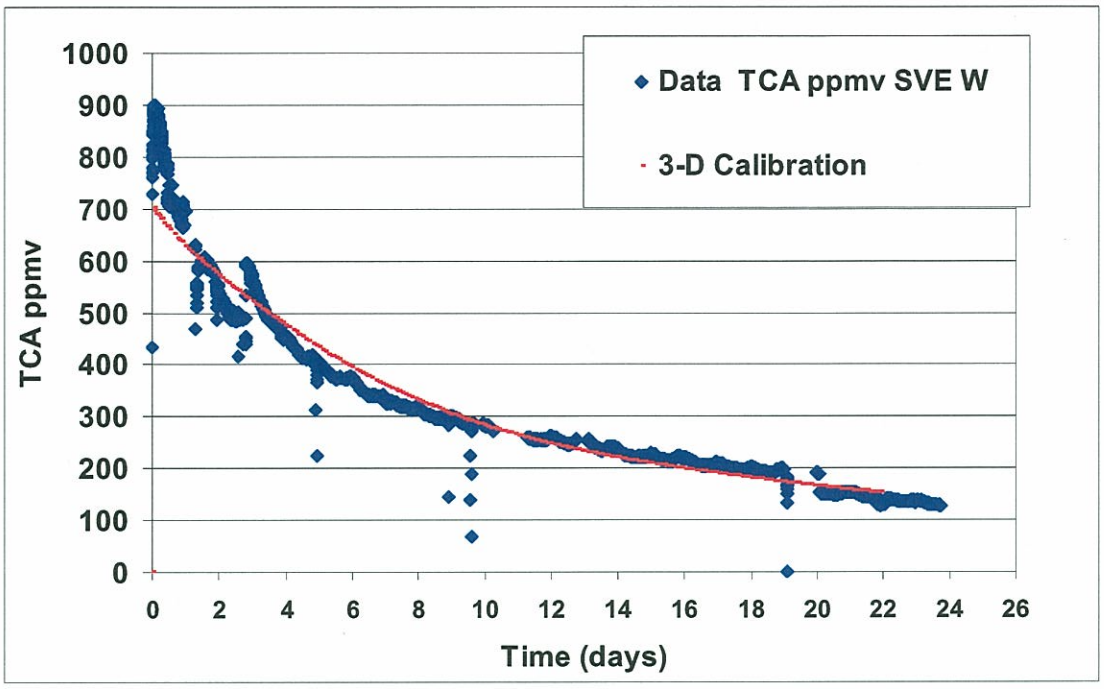

Figure 10 SVE West wellhead data versus calibrated simulation. The time period during which the SVE system was shut down for repair has been removed from the calibration.

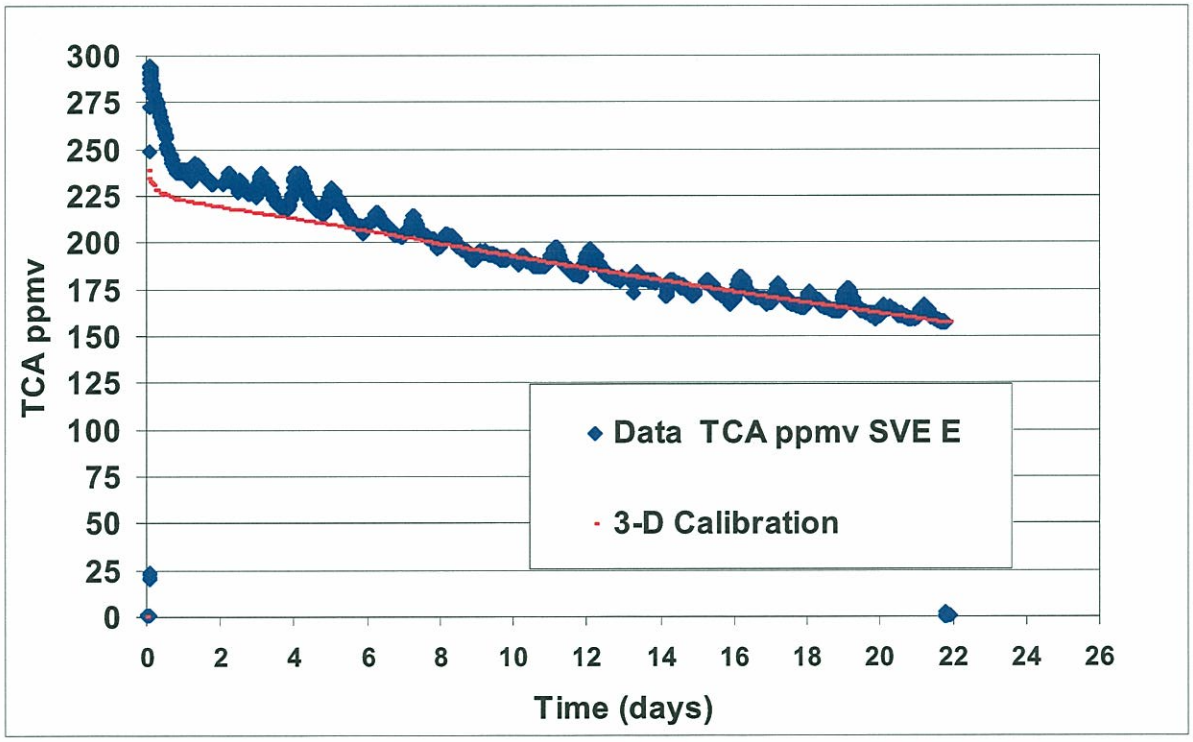

Figure 11 SVE East wellhead concentration versus time.

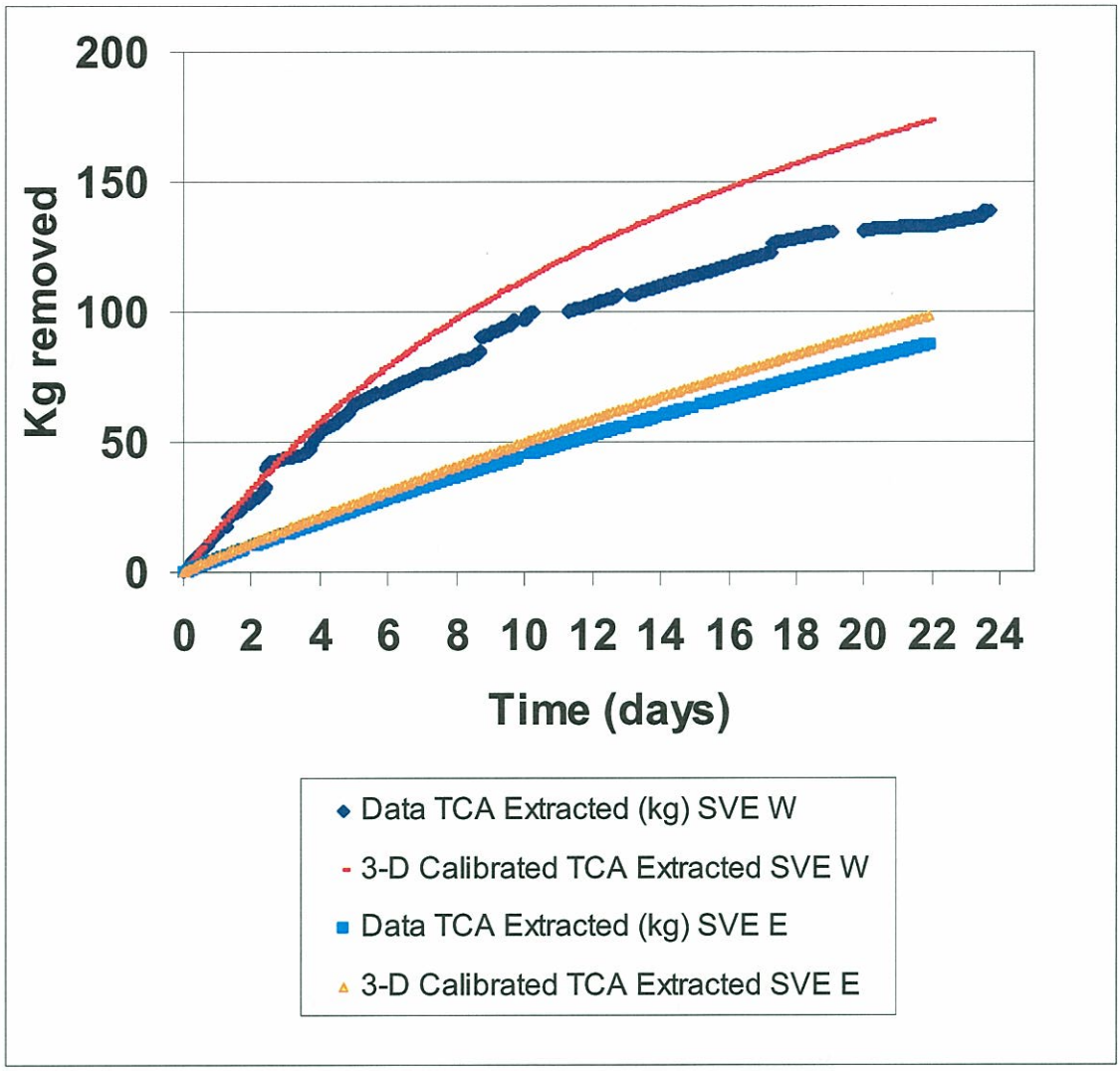

Figure 12 Mass removal for both SVE West and SVE east simulations compared to calculated mass removal rates during the Pilot Test.

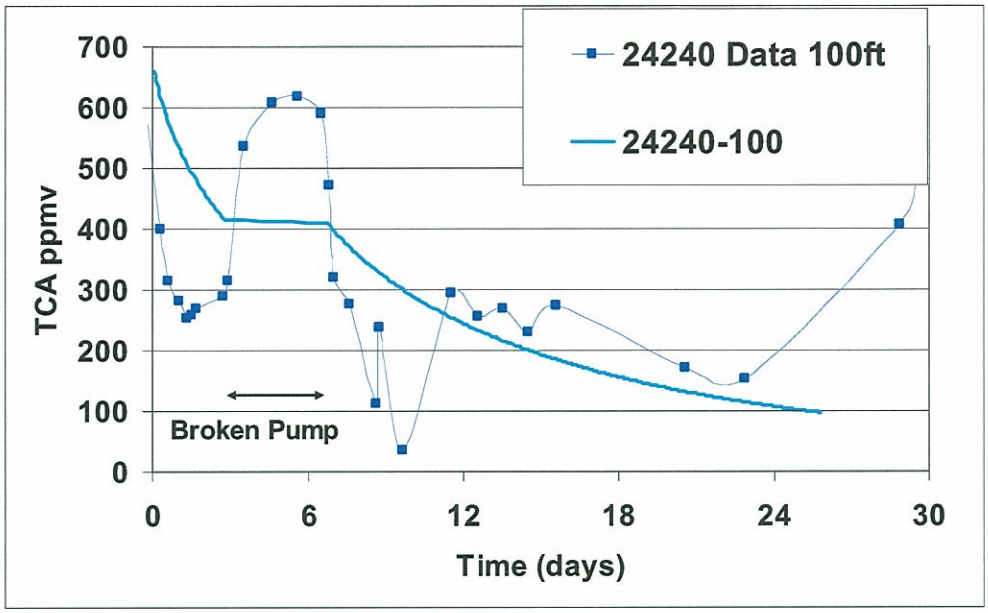

Figure 13 Concentration versus time for borehole 54-24240 at 100 ft below ground surface (bgs), model versus simulation.

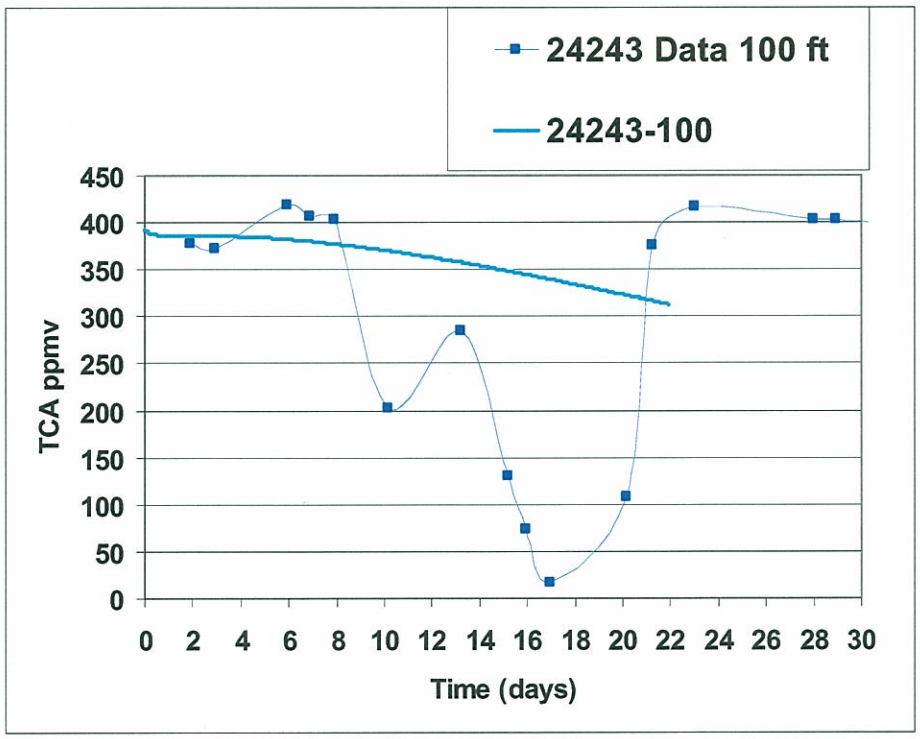

Figure 14 Concentration versus time for borehole 54-24243 at 100 ft bgs, model versus simulation.

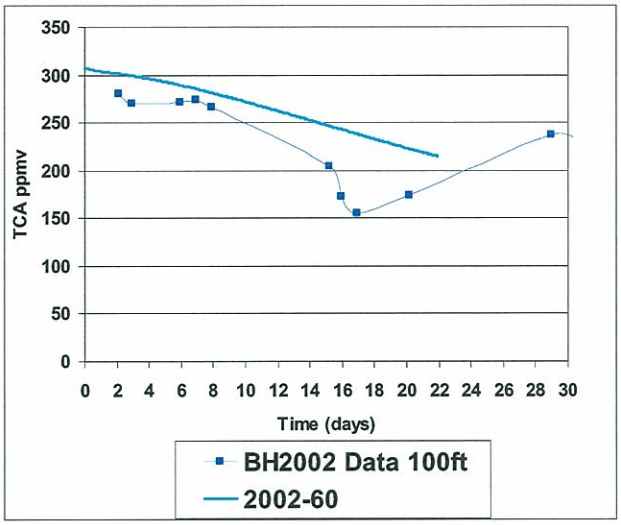

(A)

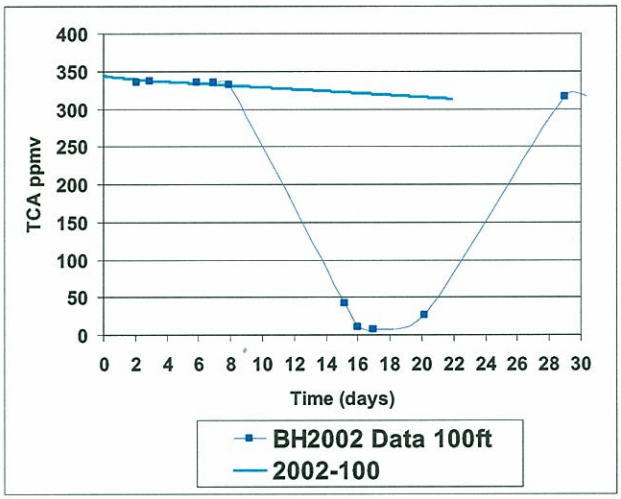

(B)

Figure 15 Concentration versus time for borehole 54-2002 at (A) 60 ft bgs and (B) 100 ft bgs, model versus simulation.

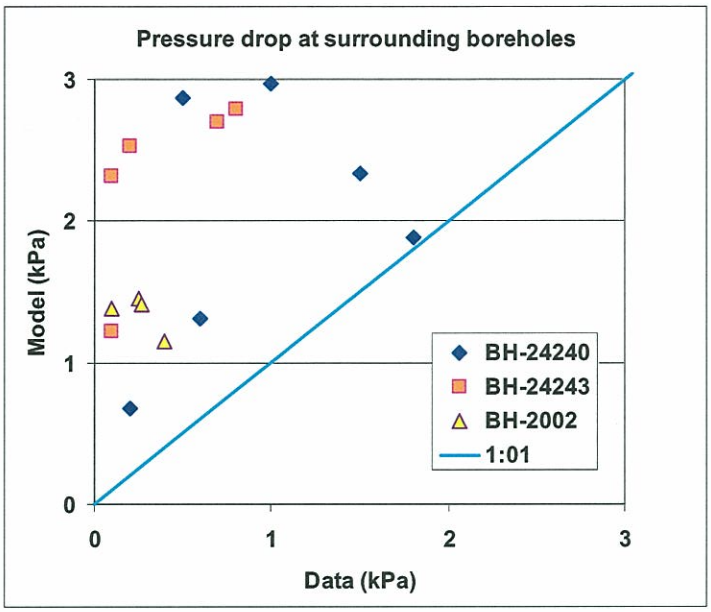

Figure 16 Manometer data versus simulation results for three boreholes. The 1:1 line is plotted to show that the simulated pressure drops are consistently higher than the measured data except for one point in BH-24240.

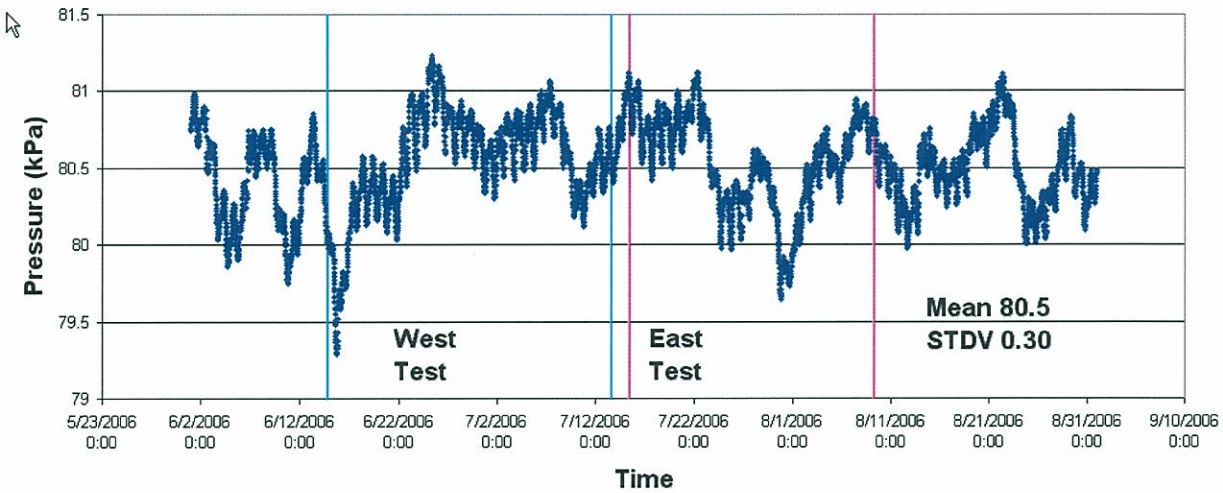

Figure 17 TA-54 barometric pressure data during the time of the SVE Pilot Test.

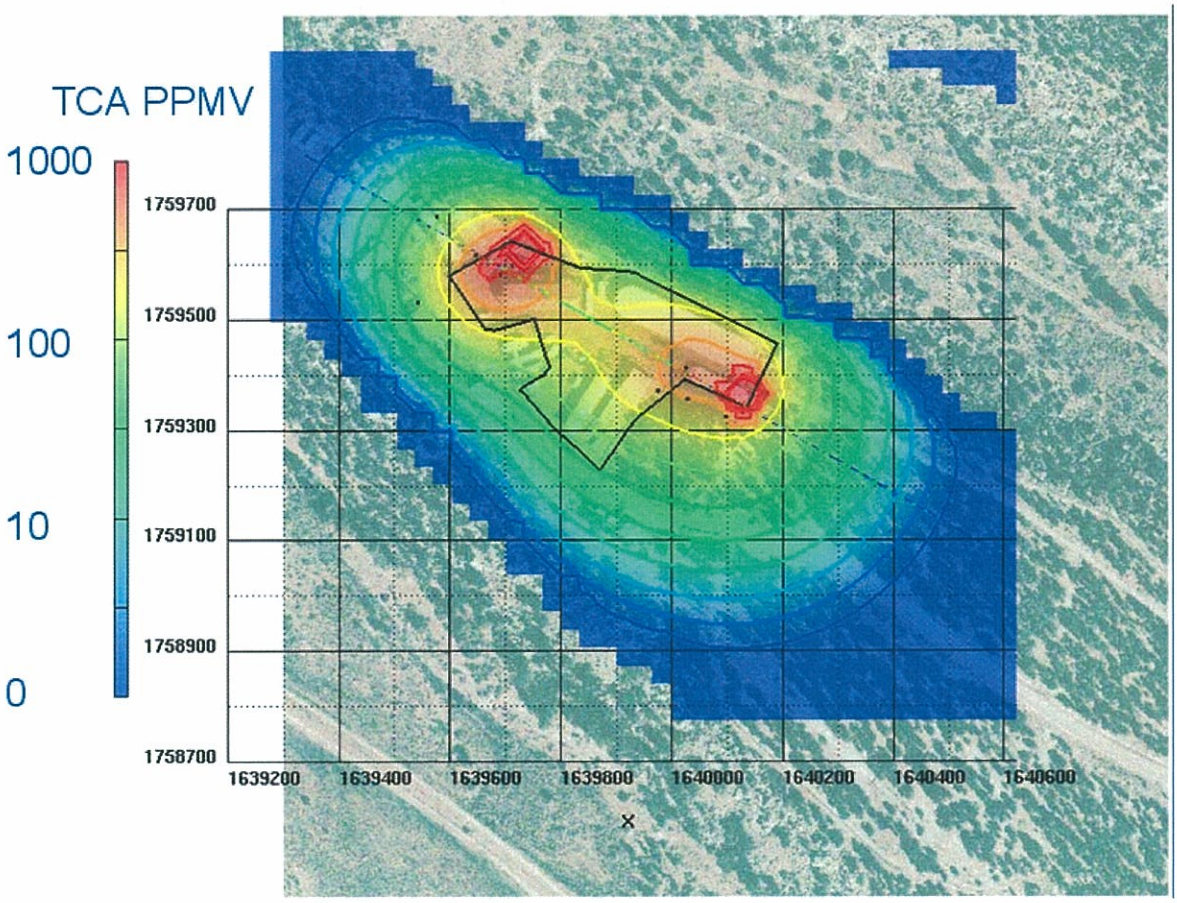

Figure 18 Source locations for the 5 drum sudden release scenario.

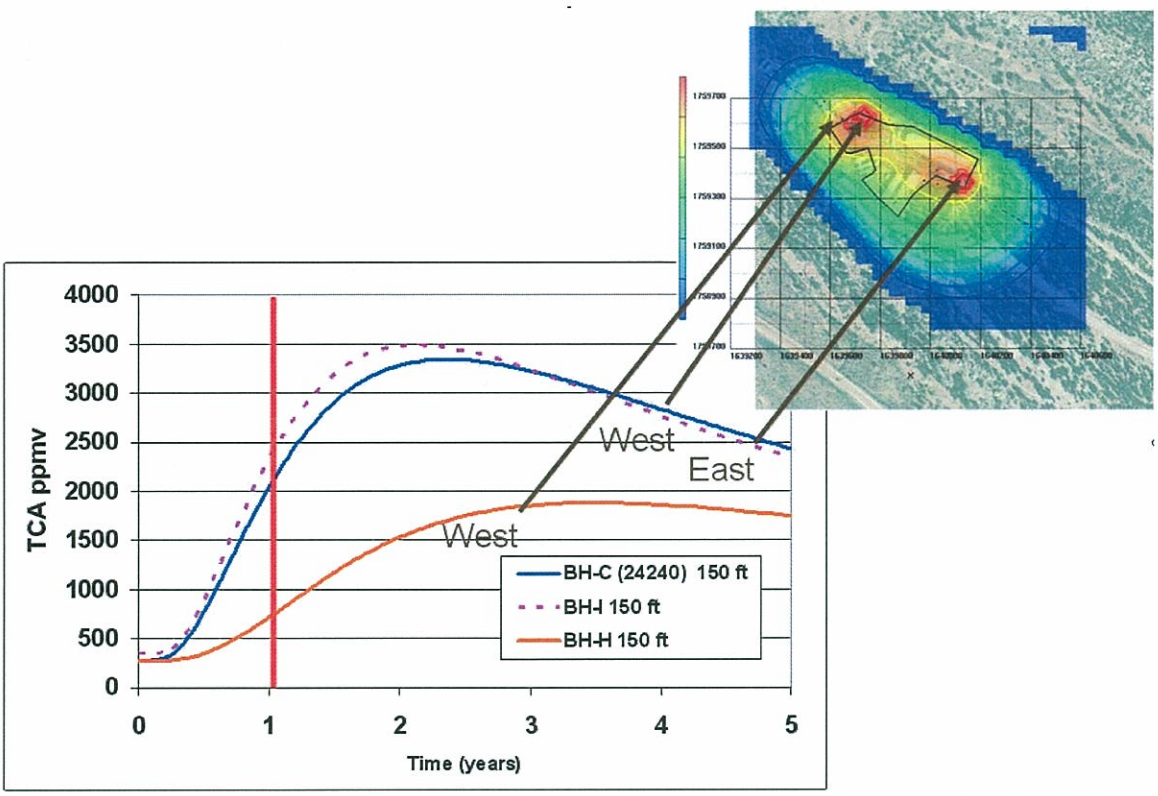

Figure 19 Response at the 150 ft. depth in several surrounding boreholes for the 5 drum release scenario.

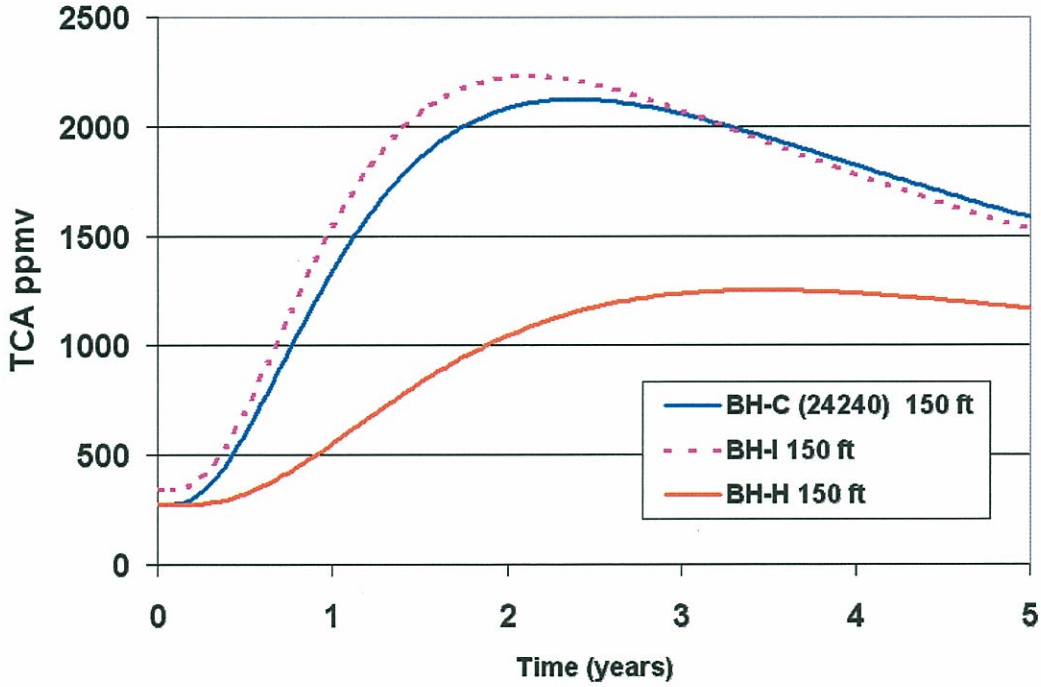

Figure 20 Response at the 150 ft. depth in several surrounding boreholes for the 3 drum release scenario.

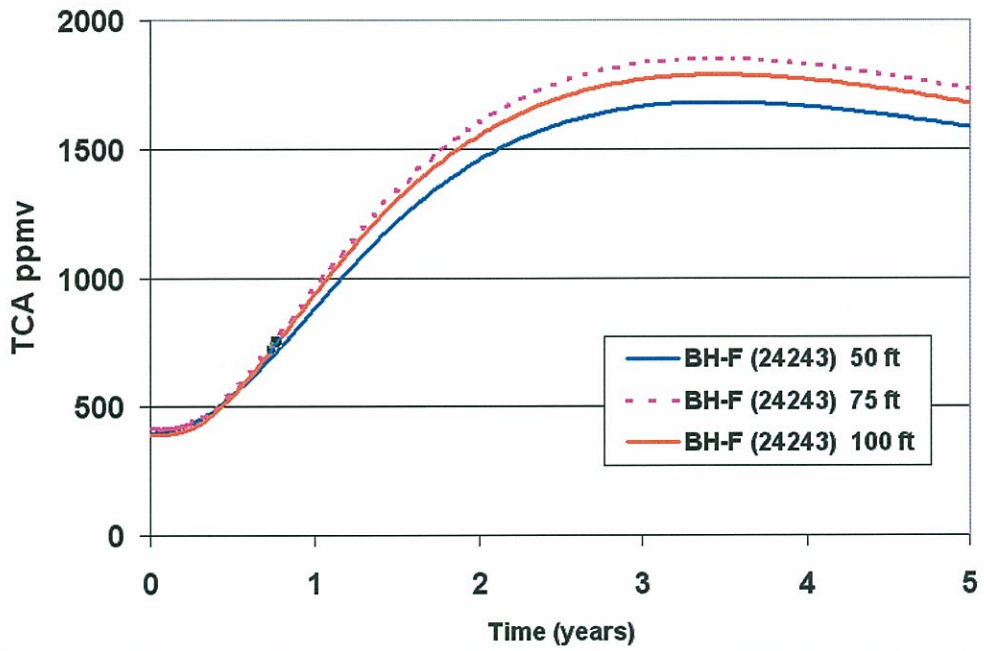

Figure 21 Concentration responses for the 5 drum scenario in boreholes E and F, located 93 ft. and 98 ft. respectively from the release area.

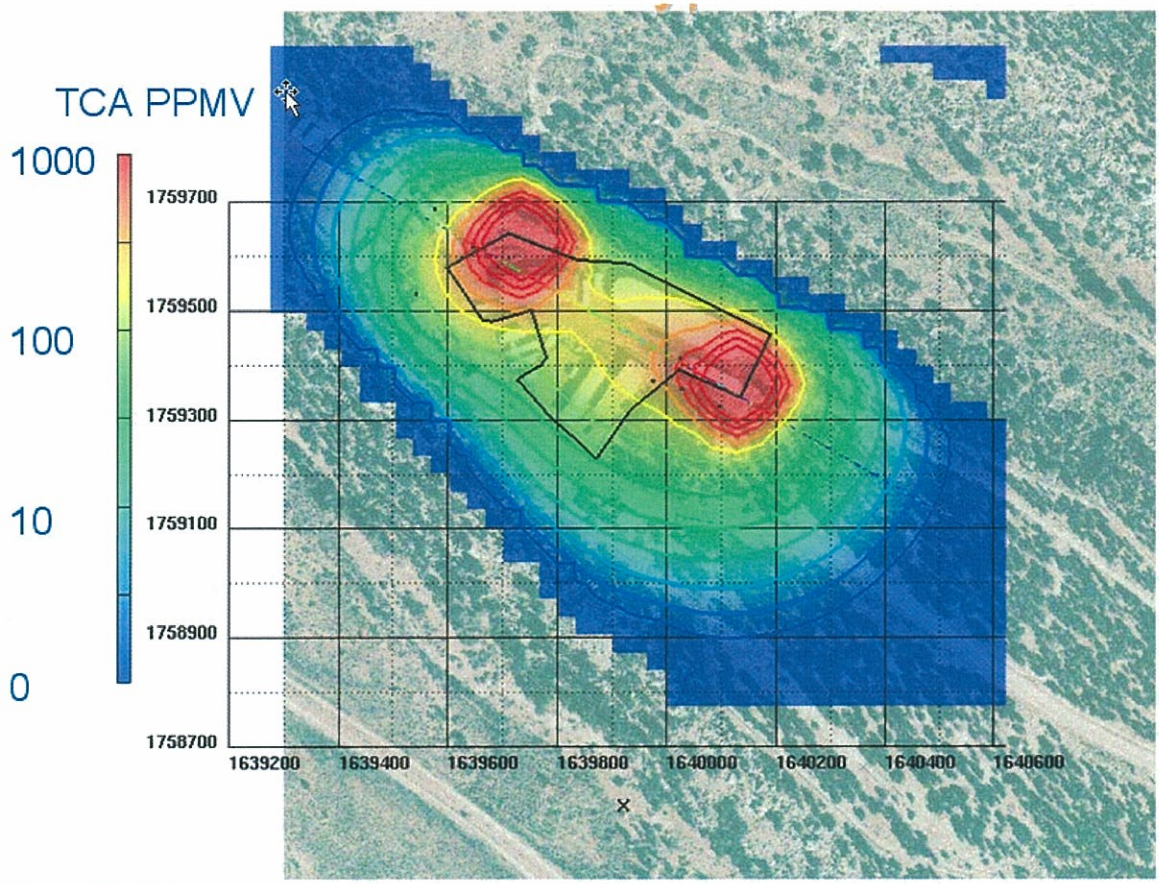

Figure 22 Concentration after one year of plume growth from the 5 drum sudden release scenario on a plane 80 ft. beneath the mesa top.

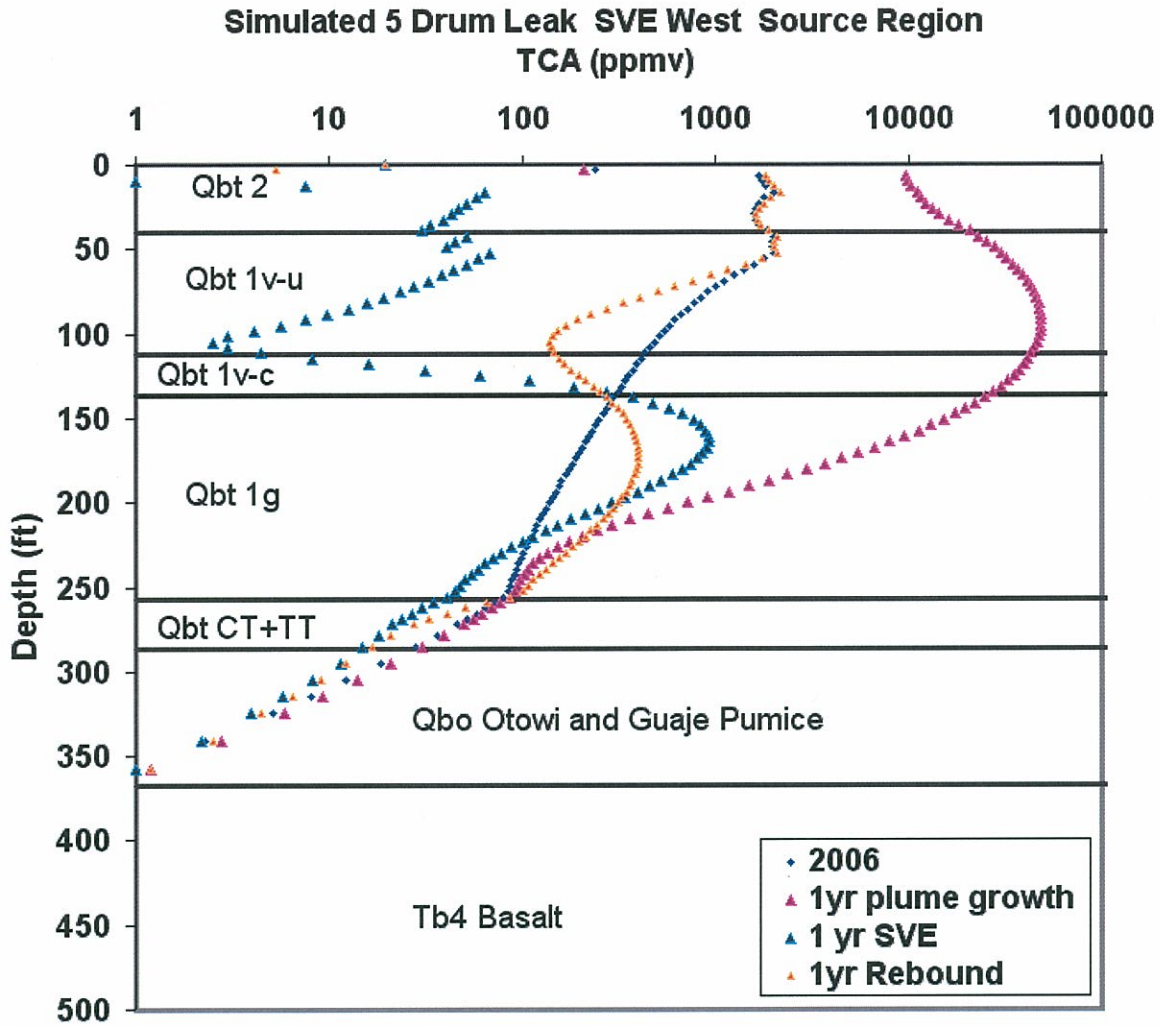

Figure 23 Concentration versus depth beneath the western sudden release area.

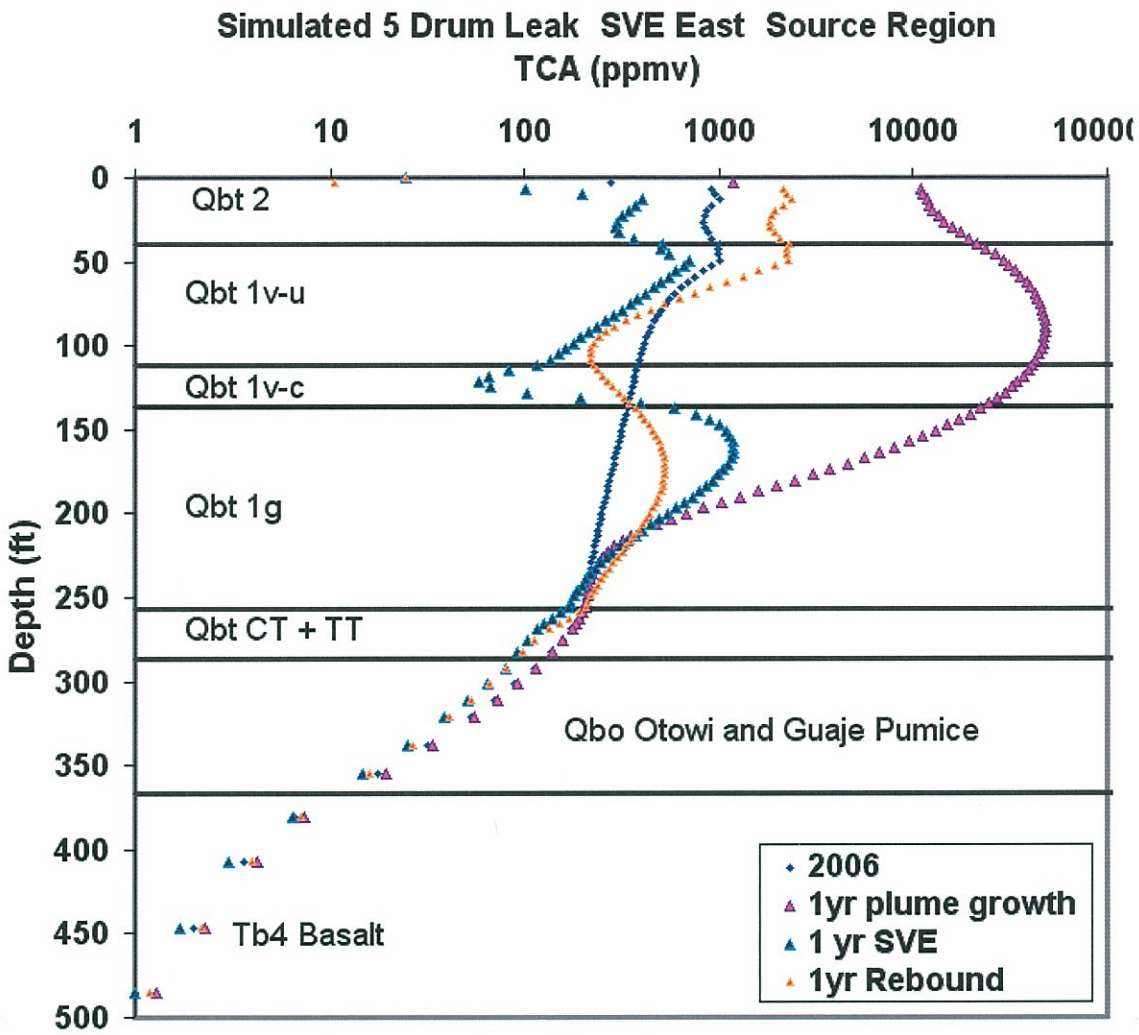

Figure 24 Concentration versus depth beneath the eastern sudden release area.

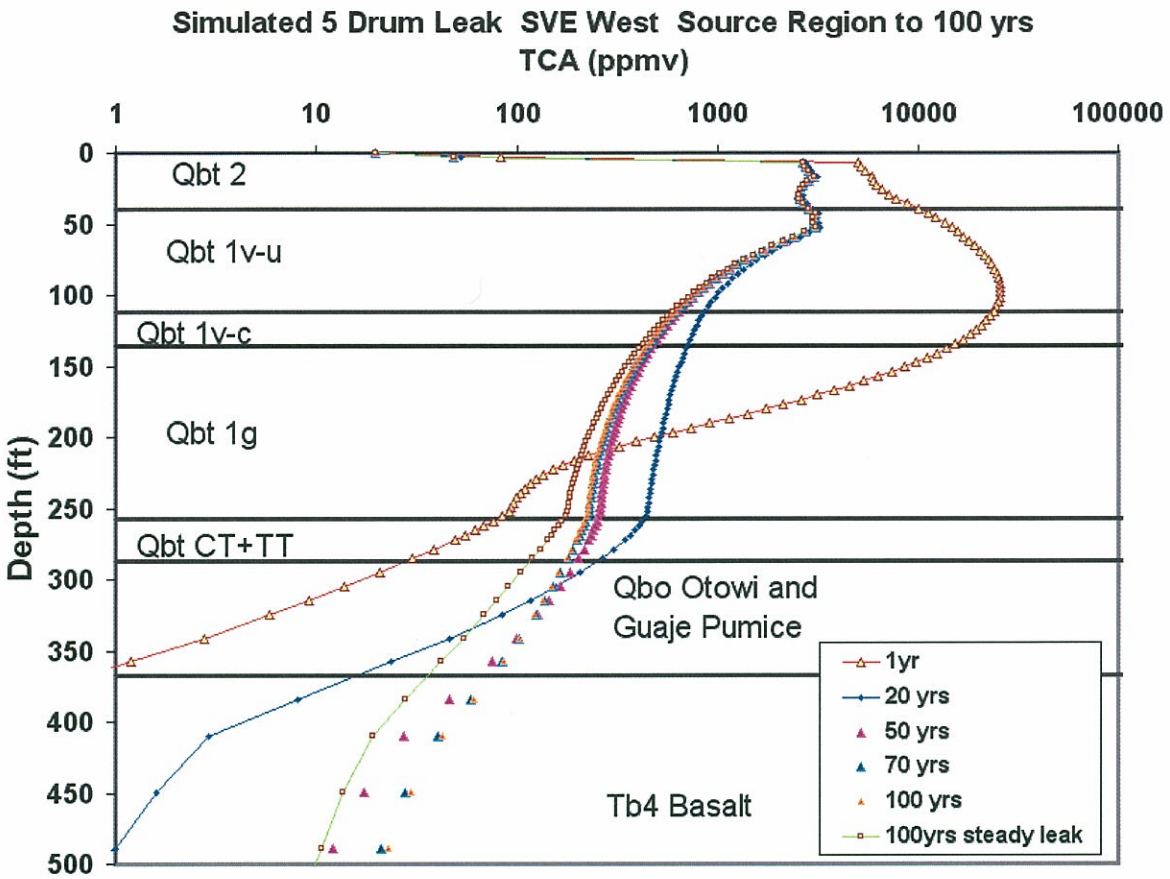

Figure 25 Concentration versus depth beneath the western sudden release area to 100 years.

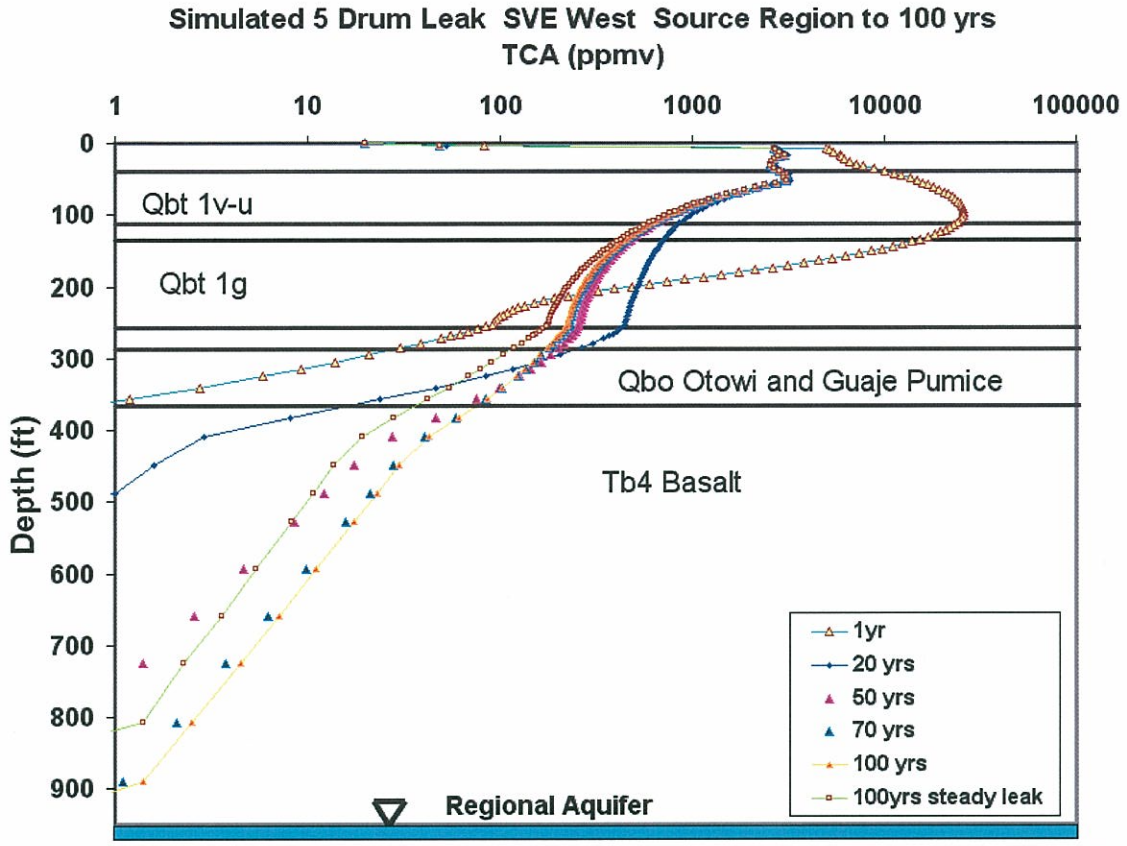

Figure 26 Concentration versus depth beneath the western sudden release area to 100 years. This figure shows the same data as in Figure 24 and also includes the depth range of the regional aquifer.

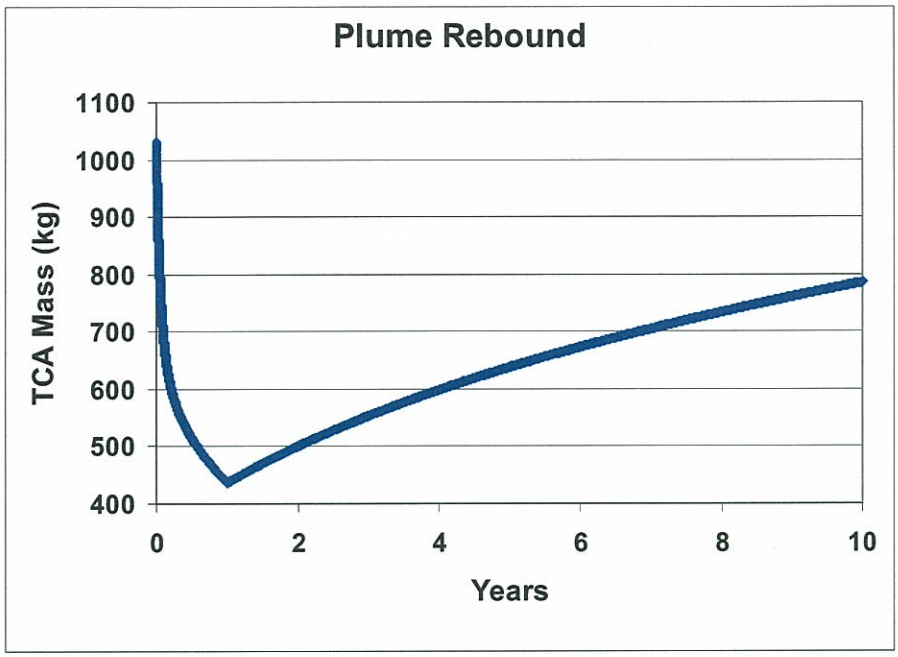

A

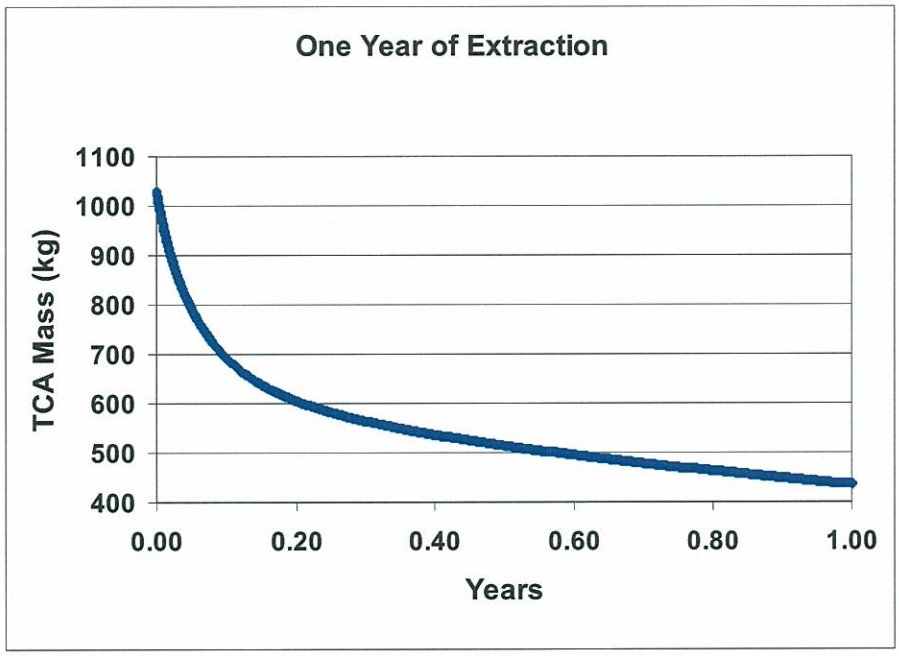

B

Figure 27 A) Plume rebound after one year of SVE. The simulation has both SVE West and East pumping for one year. After one year, both East and West source regions continue to leak at pre-SVE rates. B) Zoom in on the first year of extraction showing the change in plume mass as a function of time.

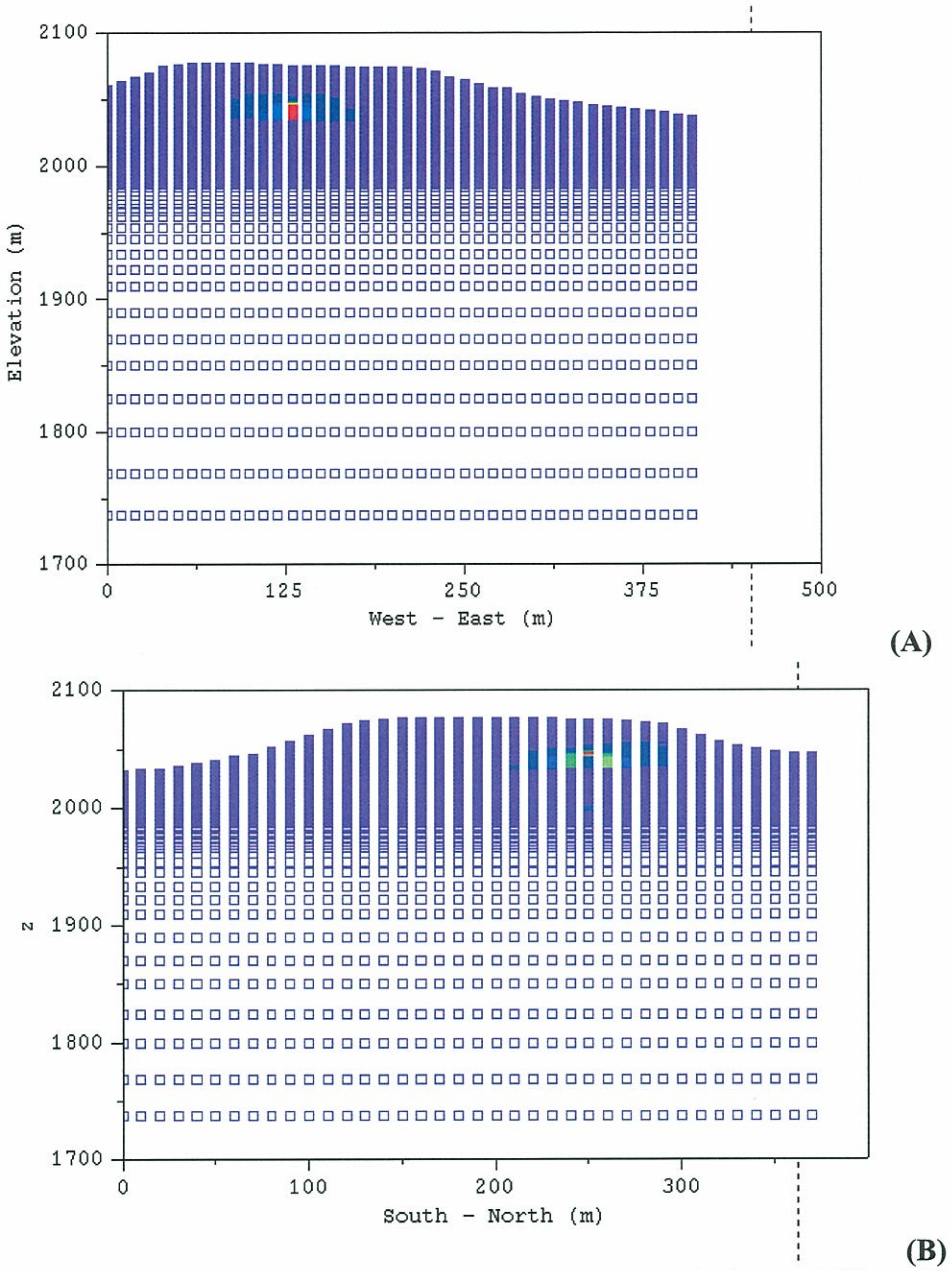

Figure 28 SVE West radius of influence on (A) a N-S slice and (B) an E-W slice, through the mesa at the SVE West location showing a region (blue to red) where the magnitude of the total volume flux is equal to or greater than 4.e-6 m/s. A particle with a volume flux of 4.e-6 m/s in a rock with porosity of 50% will move 40 m in 60 days.